Frustration shapes multi-channel Kondo physics: A Star graph perspective

Siddhartha Patra,[1,*] Abhirup Mukherjee,[1,†] Anirban Mukherjee,[1,2,‡] A. Taraphder,[3] and Siddhartha Lal[1,§]

[1] *Department of Physical Sciences, Indian Institute of Science Education and Research-Kolkata, W.B. 741246, India*
[2] *Ames Laboratory, Ames, Iowa 50011, USA*
[3] *Department of Physics, Indian Institute of Technology Kharagpur, Kharagpur 721302, India*

(Dated: January 27, 2022)

Our study of the multi-channel Kondo (MCK) model using the recently developed unitary renormalization group (URG) technique shows the importance of ground state degeneracy in explaining various important properties like the breakdown of screening and the presence of local non-Fermi liquids. The impurity susceptibility of the zero-bandwidth intermediate coupling fixed point Hamiltonian shows power-law divergence at low temperature, signaling its critical nature. Despite the absence of inter-channel coupling in the MCK Hamiltonian, the study of mutual information between two channels shows non-zero correlation among them. The presence of non-local twist and translation operators shows the topological nature of the degenerate ground state manifold. Upon disentangling the impurity spin, we find the presence of local Mott-liquid made out of inter-channel quantum scatterings. We derive the low energy effective Hamiltonian (LEH) upon the addition of excitation to the zero-bandwidth RG fixed point Hamiltonian for the two and three-channel cases, both of which show the absence of local Fermi liquid phase due to exact cancellation coming from different degenerate ground states, and the presence of non-Fermi liquids with inter-channel quantum fluctuations. Computation of various thermodynamic quantities like specific heat and susceptibility in the ground state of that non-Fermi liquid shows logarithmic scaling in low temperature, which agrees with the known result in the literature. The presence of local marginal Fermi liquid shows the orthogonality catastrophe in the two-channel Kondo model. Discontinuity in various entanglement measures as we add the excitations on top of the zero-bandwidth model by tuning the real space nearest-neighbor hopping strength reinforces the presence of orthogonality catastrophe. Strong and weak coupling duality also sheds light on the presence of an intermediate coupling fixed point in the MCK problem. The study of channel anisotropy under URG reveals series of quantum phase transitions due to the change in ground state degeneracy. Our work thus shows a template of studying the zero-bandwidth model followed by the systematic addition of excitations, which can be used to study other impurity problems.

I. INTRODUCTION

Local antiferromagnetic exchange interaction between a spin-$\frac{1}{2}$ impurity and a metal gives rise to the well-understood phenomenon of Kondo effect[1] where the impurity local moment gets screened by the conduction electrons at temperatures below a certain scale called the Kondo temperature[2–9], leading to a spin singlet ground state and local Fermi liquid excitations above that ground state[10,11]. The screening manifests as an increase in the resistivity of the metal[12,13], and in the saturation of the impurity contribution to the magnetic susceptibility[5–7], both at low temperatures. More general models are obtained by taking impurities of higher spin[1,8,14], adding interactions between them[15–21], by promoting to a Kondo lattice of impurities[22–26] or by considering a correlated metal[27]. More important to the topic at hand, one can construct multi-channel Kondo (MCK) models by allowing K channels ($K > 1$) to interact with a spin-$\frac{1}{2}$ impurity[14,28,29] via a common exchange coupling $\mathcal{J}$. Using conformal field theory[8,30–34], bosonization[35–39], numerical renormalization group[32,40,41], Bethe ansatz[42–46] and other methods[47–50], it has been shown that for the overscreened systems ($K > 2S_d$), the low energy physics is of the non-Fermi liquid type, displaying anomalous thermodynamic properties near $T = 0$ and a fractional zero temperature entropy in the thermodynamic limit (ensuring that temperature is taken to zero before the system size is taken to infinity[38,51]). This diverging behaviour is actually a signature of the fact that the system with a single channel-symmetric exchange coupling is quantum critical: it is susceptible to perturbations that introduce channel isotropy in the exchange couplings[14,32,37,45,52], rendering the realisation of such states in experiments quite a challenge. Nevertheless, several features of the two-channel Kondo model have been reproduced using structural two-level systems[28,53] interacting with a conduction bath[54–58]. More recently, it has become possible to tune a two-channel quantum dot system across the quantum phase transition[59,60], revealing the fractionalisation of the low-energy degrees of freedom[49,61,62].

The role of ground state degeneracy and quantum-mechanical frustration in the problem has not received sufficient attention, even though they play crucial role in determining the non-Fermi liquid physics and the quantum criticality of the system. This is, at least partially, due to the lack of an intermediate-coupling effective Hamiltonian that describes the low-energy physics of the MCK and reveals the channel non-diagonal nature of the excitations. The frustration in this context is the inability of the impurity spin to bind with a single conduction channel and form a maximally-entangled singlet. The absence of such frustration in the single-

channel model means that drastic differences should exist compared to the multi-channel models at inexact screening ($K \neq 2S_d$). Indeed, we show later that the orthogonality catastrophe in the MCK models is one such difference and that it is directly related to the degenerate ground state manifold. Another place where the effects of the non-diagonal low energy excitations are expected to show up is many particle entanglement, but the lack of an intermediate coupling Hamiltonian has prevented the study of entanglement as a function of the RG flow[63,64]. Our effective Hamiltonian as well as the specific method enables the calculation and comparison of such measures of entanglement (for eg., the inter-channel mutual information) along the RG flow and as functions of the excitation energies, providing insight into the nature of the fixed point theory.

To obtain the RG flow of the MCK model, we have employed the recently developed unitary renormalization group (URG) technique[65,66]. The method has been applied on several fermionic and spin problems like the single-channel Kondo model[67], the kagome antiferromagnet[68], the 1D[69] and 2D Hubbard models[70,71], the reduced-BCS model[72] as well as other generalised models of interacing electrons with and without translation invariance[66]. The URG proceeds by decoupling number fluctuations in the high energy electronic states. Iteratively applying this URG method on the channel-isotropic MCK model leads to a low energy fixed point Hamiltonian at intermediate Kondo coupling. Initially we focus on the zero bandwidth limit of this Hamiltonian and show that most important properties of the MCK problem like ground state degeneracy and breakdown of screening can be understood from this zero bandwidth problem. We then go on to study the role of excitations and derived the low energy effective Hamiltonian for the non-Fermi liquid excitations. Such a Hamiltonian enables the computation of a plethora of quantities like the thermodynamic measures (like specific heat and susceptibility), many-particle entanglement and self-energy. We also explore various signatures of criticality and the possibility of duality transformations of the MCK Hamiltonian. Finally, we take a look at the channel anisotropic MCK model to determine its RG flows and the change in ground state degeneracy on account of the degeneracy. The main results and the layout of the work is summarised below.

Summary of Main Results

We start in section II where we describe, in detail, the URG flows, the intermediate coupling URG fixed point Hamiltonian and the features of the zero bandwidth limit of the effective Hamiltonian. In section III, we explore some properties of the zero bandwidth model: the degree of compensation, impurity magnetisation and impurity susceptibility. The degree of compensation is simply the average correlation between the impruity spin and the conduction channel local spins; it is found to be maximum at exact screening and decreases for both over- and under-screening. It is therefore a quantitative measure of the breakdown of screening away from exact screening. The magnetisation and susceptibility show critical behaviour in the form a discontinuity and a T^{-1} divergence respectively. To complete the study of the zero bandwidth model, we recreate the degenerate ground-state manifold using non-local twist and translation operators. On decoupling the impurity spin from the local conduction spin degrees of freedom, we obtain an all-to-all Hamiltonian that represents a local Mott liquid phase. In IV, we obtain the low energy effective Hamiltonian for the excitations brough about by the real space tight-binding hopping into the lattice. Notable features include the complete absence of local Ferm liquid terms and the emergence of local non-Fermi liquid terms, both being results of the ground state degeneracy. The excitations are found to contain a marginal Fermi liquid, signaling an orthogonality catastrophe in the two-channel Kondo problem. In section V, we study various entanglement signatures of the low energy fixed-point ground state of the MCK problem. Firstly, we study various entanglement properties like the von-Neumann entanglement entropy of the impurity with the rest, mutual information, and multi-partite information scaling of the zero bandwidth (star graph) model. We also show the variation of various entanglement measures (impurity entanglement entropy, mutual information, Bures distance) as the hybridisation with the lattice is increased. In VI we discuss two duality transformations that exist for the MCK model. The strong-weak duality relates an MCK at strong-coupling to another at weak-coupling, and it is shown that the presence of a unique intermediate coupling fixed point constrains the nature of the transformation. The other duality transformation is between underscreened and overscreened models, and it implies that if the strong-coupling fixed point is unstable in the overscreened model, it is bound to be stable in the underscreened model. In VII we show the robustness of the star graph ground state degeneracy against the impurity-channel coupling anisotropy, and follow it up with a URG treatment of the channel anisotropic MCK; the isotropic fixed point is found to be unstable to asymmetry, leading to impurity phase transitions driven by channel anisotropy.

II. FIXED POINT THEORY OF OVER-SCREENED MULTI-CHANNEL KONDO MODEL

A. RG flows towards intermediate coupling

We start with the usual K-channel Kondo model Hamiltonian with isotropic couplings[14]. $\mathcal{J}$ is the Kondo spin-exchange coupling. $c_{k\alpha,l}$ is the fermionic field operator at momentum k, spin α and channel l. $\epsilon_{k,l}$ represents

the dispersion of the l^{th} conduction channel. $\vec{\sigma}$ is the vector of Pauli matrices and $\vec{S}_d = \frac{1}{2}\vec{\sigma}_d$ is the impurity spin operator.

$$H = \sum_l \Bigg[\sum_{\substack{k \\ \alpha=\uparrow,\downarrow}} \epsilon_{k,l}\hat{n}_{k\alpha,l} + \frac{\mathcal{J}}{2} \sum_{\substack{kk' \\ \alpha,\beta=\uparrow,\downarrow}} \vec{S}_d \cdot \vec{\sigma}_{\alpha\alpha'} c^\dagger_{k\alpha,l} c_{k'\alpha',l} \Bigg] . \tag{1}$$

Here, l sums over the K channels of the conduction bath, k, k' sum over all the momentum states of the bath and α, β sum over the two spin indices of a single electron.

We have performed a renormalisation group analysis of the Hamiltonian using the recently developed URG method[65,66,68–72]. The RG proceeds by applying unitary transformations in order to block-diagonalize the Hamiltonian by removing number fluctuations of the high energy degrees of freedom. If the most energetic electronic state at the j^{th} RG step is $|j\rangle$ defined by the energy $D_{(j)}$, the Hamiltonian will in general not conserve the number of particles in this state: $\left[H_{(j)}, \hat{n}_j\right] \neq 0$. The unitary transformation $U_{(j)}$ will remove this number fluctuation at the next RG step[65,66]:

$$H_{(j-1)} = U_{(j)} H_{(j)} U^\dagger_{(j)}, \;\; \left[H_{(j-1)}, \hat{n}_j\right] = 0 \tag{2}$$

The unitary transformations are given in terms of a fermionic generator $\eta_{(j)}$[65,66]:

$$U_{(j)} = \frac{1}{\sqrt{2}} \left(1 + \eta_{(j)} - \eta^\dagger_{(j)}\right), \quad \left\{\eta_{(j)}, \eta^\dagger_{(j)}\right\}_\pm = 1 \tag{3}$$

where $\{A, B\}_\pm = AB \pm BA$. The generator itself is given by the expression[65,66]

$$\eta^\dagger_{(j)} = \frac{1}{\hat{\omega}_{(j)} - \text{Tr}\left(H_{(j)}\hat{n}_j\right)} c^\dagger_j \text{Tr}\left(H_{(j)} c_j\right) \tag{4}$$

The operator $\hat{\omega}_{(j)}$ encodes the quantum fluctuation scales arising from the interplay of the kinetic energy terms and the interaction terms of the Hamiltonian:

$$\hat{\omega}_{(j)} = H_{(j-1)} - H^i_{(j)} \tag{5}$$

$H^i_{(j)}$ is that part of $H_{(j)}$ that commutes with $\hat{n}_j$ but does not commute with at least one $\hat{n}_l$ for $l < j$. The RG continues up to energy D^* where a fixed point is reached from the vanishing of either the numerator or the denominator.

The derivation of the RG equation for the over-screened regime ($2S < K$) of the spin-S-impurity K-channel Kondo problem is shown in detail in the supplementary materials. On decoupling circular isoenergetic shells at energies $D_{(j)}$, the change in the Kondo coupling at the j^{th} RG step, $\Delta\mathcal{J}_{(j)}$, is given by

$$\Delta\mathcal{J}_{(j)} = -\frac{\mathcal{J}^2_{(j)}\mathcal{N}_{(j)}}{\omega_{(j)} - \frac{D_{(j)}}{2} + \frac{\mathcal{J}_{(j)}}{4}} \left(1 - \frac{1}{2}\rho\mathcal{J}_{(j)}K\right) \tag{6}$$

$\mathcal{N}_{(j)}$ is the number of electronic states at the energy shell $D_{(j)}$. We work in the low quantum fluctuation regime $\omega_{(j)} < \frac{D_{(j)}}{2}$. There are three fixed points of the RG equation. One arises from the vanishing of the denominator, and was present in the single-channel Kondo RG equation as well[67]. As shown there, this fixed-point goes to $\mathcal{J}^* = \infty$ as the bare bandwidth of the conduction electrons is made large. The other trivial fixed point is the trivial one at $\mathcal{J}^* = 0$. The third fixed point is reached when the numerator vanishes: $\mathcal{J}^* = \frac{2}{K\rho}$[14,73–75]. Only the intermediate fixed point is found to be stable. This is consistent with results from Bethe ansatz calculations[42–46,76], CFT calculations[8,30,31], bosonization treatments[35,38] and NRG analysis[41,77].

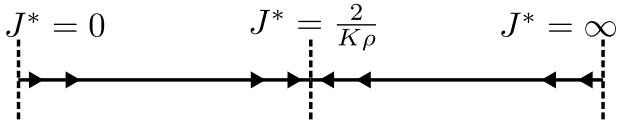

FIG. 1. The three fixed points of the over-screened RG equation. Only the intermediate one is stable.

The RG equation reduces to the perturbative form $\Delta\mathcal{J}_{(j)} \simeq \frac{\mathcal{J}^2_{(j)}\mathcal{N}_{(j)}}{D_{(j)}} \left(1 - \frac{1}{2}\rho\mathcal{J}_{(j)}K\right)$[14,74,75,78] when one replaces $\omega_{(j)}$ with the ground state energy $-\frac{D_{(j)}}{2}$ and assumes $\mathcal{J} \ll D_{(j)}$.

B. The star graph as the zero-bandwidth limit of the fixed point Hamiltonian

The fixed point Hamiltonian takes the form

$$H^* = \sum_l \left[\sum_k^* \epsilon_{k,l}\hat{n}_{k\alpha,l} + \mathcal{J} \sum_{kk'}^* \vec{S}_d \cdot \frac{1}{2}\vec{\sigma}_{\alpha\alpha'} c^\dagger_{k\alpha,l} c_{k'\alpha',l} \cdot \right] \tag{7}$$

We have not explicitly written the decoupled degrees of freedom $D_{(j)} > D^*$ in the Hamiltonian. The $*$ over the summations indicate that only the momenta inside the window D^* enter the summation. There is an implied summation over the spin indices α, β.

We will first study the zero bandwidth limit of the fixed point Hamiltonian, obtained by compressing the sum over the momentum states to a single state at the Fermi surface. Upon setting the chemical potential equal to the Fermi energy, the kinetic energy part vanishes and the zero bandwidth model becomes a Heisenberg spin-exchange Hamiltonian.

$$H^* = \mathcal{J} \sum_l \sum_{kk'}^* \vec{S}_d \cdot \frac{1}{2}\vec{\sigma}_{\alpha\alpha'} c^\dagger_{k\alpha,l} c_{k'\alpha',l} = \mathcal{J}\vec{S}_d \cdot \vec{S} \; . \tag{8}$$

At the last step, we defined the total bath local spin operator $S = \sum_l \vec{S}_l = \frac{1}{2}\sigma_l = \frac{1}{2}\sum_{kk'}^* \sum_{\alpha\beta} \vec{\sigma}_{\alpha\alpha'} c^\dagger_{k\alpha,l} c_{k'\alpha',l}$. The star graph commutes with several operators, includ-

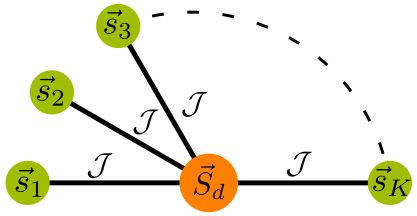

FIG. 2. Zero bandwidth limit of the fixed point Hamiltonian. The central yellow node is the impurity; it is interacting with the K green outer nodes that represent the local spins of the channels.

ing the total spin operator $J^z = S_d^z + S^z$ along z, the total bath local spin operator S^2 and the string operators

$$\pi^{x,y,z} = \sigma_d^{x,y,z} \otimes_{l=1}^{K} \sigma_l^{x,y,z} \ . \tag{9}$$

If we define the global spin operator $\vec{J} = \vec{S} + \vec{S}_d$, the star graph Hamiltonian can be written as $\mathcal{J}\left[J^2 - S_d^2 - S^2\right]$. The ground state is achieved for the maximal value of S, $S = \frac{K}{2}$, and the corresponding minimal value of J, $J = |\frac{K}{2} - S_d|$. This value corresponds to a multiplicity of $2J+1 = |K - 2S_d| + 1$ in J^z, and since the Hamiltonian does not depend on J^z, these orthogonal states $|J^z\rangle$ constitute a degeneracy of $g_K^{S_d} = |K - 2S_d| + 1$.

The π^z acts on the eigenstates $|J^z\rangle$ and reveals the odd-even parity of the eigenvalue J^z, and is hence a parity operator. Interestingly, the string operator π^z is a Wilson loop operator[79] that wraps around all the nodes of the star graph:

$$\pi^z = \exp\left[i\frac{\pi}{2}\left(\sigma_d^z + \sum_{l=1}^{K}\sigma_l^z - K\right)\right] = e^{i\pi\left(J^z - \frac{1}{2}K\right)} \tag{10}$$

π^x and π^y are 't Hooft operators[79] and mix states of opposite parity. For example, it can be shown that $\pi^x |J^z\rangle = -|J^z\rangle$.

There are good reasons for working with the star graph in particular and zero mode Hamiltonians in general. In the single-channel Kondo model, the star graph is just the two spin Heisenberg, and it reveals the stabilization of the Kondo model ground state, as well as certain thermodynamic properties (e.g., the impurity contribution to the susceptibility)[67,80–83]. Similarly in the MCK model, the star graph is able to mimic the nature of the RG flows. At weak coupling $\mathcal{J} \to 0^+$, the central spin is weakly coupled to the outer spins and prone to screening because of the $S^{\pm}$ terms in the star graph; at strong coupling $\mathcal{J} \to \infty^-$, the outer spin-half objects tightly bind with the central spin-half object to form a single spin object that interacts with the remaining states through an exchange coupling which is RG relevant. This renders both the terminal fixed points unstable. The true stable fixed point must then lie somewhere in between, and we recover the schematic phase diagram of fig. 1.

Moreover, the RG flows of the MCK model have been show to preserve the degeneracy of the ground state[41,84,85], and the star graph captures this degeneracy in its entirety. This is important, because it will be shown in a later section that the lowest excitations of the intermediate fixed point is described a non-Fermi liquid phase, and it can be argued that this non-Fermi liquid physics arises solely from the ground state degeneracy of the underlying zero mode Hamiltonian. As mentioned previously, the ground state degeneracy of the more general star graph with a spin-S_d impurity and K channels is given by $g_K^{S_d} = |K - 2S_d| + 1$. The cases of $K = 2S_d$, $K < 2S_d$ and $K > 2S_d$ correspond to exactly screened, under-screened and over-screened regimes respectively. The latter two cases correspond to a multiply-degenerate manifold $g_K^S > 1$, and simultaneously have non-Fermi liquid phases[8,14,30,33,35,49,73,76,86–94], while the first regime has a unique ground state $g_K^S = 1$ and is described by a local Fermi liquid (LFL) phase[5–7,10,14], thereby substantiating the claim that a degeneracy greater than unity is closely tied to non-Fermi liquid physics.

In the following sections, we will show how the inherent quantum-mechanical frustration of singlet order that is present in the Hamiltonian leads to the non-trivial physics of the fixed points in terms of non-Fermi liquid phase, diverging thermodynamic quantities, quantum criticality as well as emergent gauge theories.

III. IMPORTANT PROPERTIES OF THE STAR GRAPH

A. Degree of compensation: a measure of the frustration

One can quantify the amount of screening of the local moment at the impurity site by defining a degree of compensation κ. Such a quantity also measures the inherent singlet frustration in the problem: the higher the degree of compensation, the better the spin can be screened into a singlet and lower is the frustration. It is given by the antiferromagnetic correlation existing between the impurity spin and conduction electron channels: $\Gamma \equiv -\left\langle \vec{S}_d \cdot \vec{S} \right\rangle$. The expectation value is calculated in the ground state. Since the inner product is simply the ground state energy of a spin-S impurity $K-$channel MCK model in units of the exchange coupling J, we have

$$\Gamma = \frac{1}{2}\left[l_{\text{imp}}^2 + l_c^2 - g_K^S\left(g_K^S - 1\right)\right] \tag{11}$$

$l_{\text{imp}}^2 = S_d(S_d+1)$ is the length-squared of the impurity spin. Similarly, $l_c^2 = \frac{K}{2}\left(\frac{K}{2}+1\right)$ is the length-squared of the total conduction bath spin. $g_K^S = |K - S_d| + 1$ is the ground state degeneracy. We will explore the three regimes of screening by defining $K = K_0 + \delta, S = \frac{K_0}{2} - \delta$. $\delta = 0$ represents the exactly-screened case of $K = 2S = K_0$. Non-zero δ represents either over- or under-screening. In terms of K_0 and δ, the degree of

compensation becomes

$$\Gamma = \frac{1}{4}\left[(K_0+1)^2 - (|\delta|+1)^2\right] \tag{12}$$

For a given K_0, the degree of compensation is maximised for exact screening $\delta = 0$, and is reduced for $\delta \neq 0$. This shows the inability of the system to form a unique singlet ground state and reveals the quantum-mechanical frustration inherent in the zero mode Hamiltonian and therefore in the entire problem. The degree of compensation is symmetric under the Hamiltonian transformation $\delta \to -\delta$, and this represents a duality transformation between over-screened and under-screened MCK models. This topic will be discussed in more detail later.

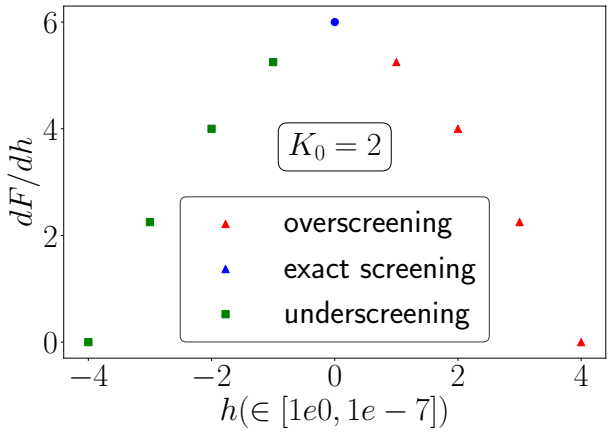

FIG. 3. Variation of the degree of compensation as we tune the system from under-screening to over-screening. The maximum spin compensation occurs at exact-screening $\delta = 0$.

B. Impurity magnetization and susceptibility

In order to obtain the magnetic susceptibility, We insert a magnetic field that acts only on the impurity and then diagonalize the Hamiltonian.

$$H(h) = \mathcal{J}^* \vec{S}_d \cdot \vec{S} + h S_d^z \tag{13}$$

The Hamiltonian commutes with S, so it is already block-diagonal in terms of the eigenvalues M of S. M takes values in the range $[M_{\min}, M_{\max}]$, where $M_{\max} = K/2$ for a $K-$channel Kondo model, and $M_{\min} = 0$ if K is even, otherwise $\frac{1}{2}$. Defining $\alpha = \frac{1}{2}(\mathcal{J}m + h) + \frac{\mathcal{J}}{4}$ and $x_m^M = M(M+1) - m(m+1)$, the partition function can be written as

$$Z(h) = \sum_{M=M_{\min}}^{M_{\max}} r_M^K \Bigg[\sum_{\substack{m=-M,\\ m\in\mathbb{Z}}}^{M-1} 2e^{\beta\frac{\mathcal{J}}{4}} \cosh\beta\sqrt{\mathcal{J}^2 x_m^M/4 + \alpha^2} + 2e^{-\beta\mathcal{J}M/2}\cosh\beta h/2 \Bigg] \tag{14}$$

Here, $\beta = \frac{1}{k_B T}$, M sums over the eigenvalues of S while m sums over $\mathcal{J}^z - \frac{1}{2}$ and the additional degeneracy factor $r_M^K = {}^{K-1}C_{K/2-M}$ arises from the possibility that there are multiple subspaces defined by $S = M$. To calculate the impurity magnetic susceptibility, we will use the expression

$$\chi = \frac{1}{\beta}\lim_{h\to 0}\left[\frac{Z''(h)}{Z(h)} - \left(\frac{Z'(h)}{Z(h)}\right)^2\right] \tag{15}$$

where the $'$ indicates derivative with respect to h. For brevity, we define $\theta_M = \beta\mathcal{J}(M+\frac{1}{2})/2$ and $\Sigma_M = \sum_{\substack{m=-M,\\ m\in\mathbb{Z}}}^{M-1}(m+\frac{1}{2})^2$. At low temperatures, the derivatives are

$$Z \to 2r_{M_{\max}}^K M_{\max} e^{\beta\frac{J}{2}(M_{\max}+1)} \tag{16}$$

$$Z'' \to r_{M_{\max}}^K \left(\frac{\beta}{2(M_{\max}+\frac{1}{2})}\right)^2 e^{\beta\frac{J}{2}(M_{\max}+1)}\Sigma_{M_{\max}} \tag{17}$$

$$\chi \to \frac{\beta\Sigma_{\max}}{2M_{\max}(2M_{\max}+1)^2} = \frac{\beta(K-1)}{12(K+1)} \sim \frac{1}{T} \tag{18}$$

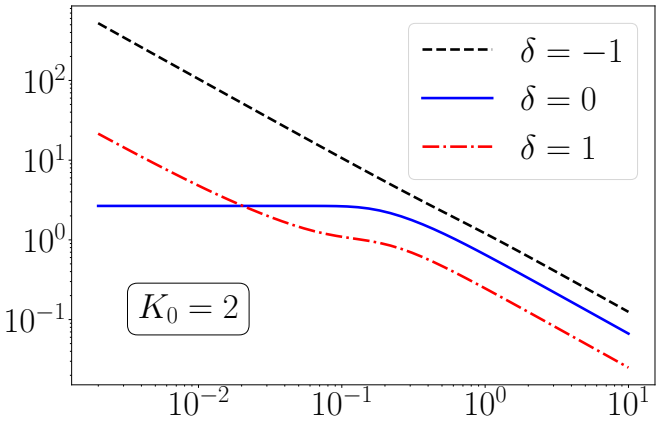

FIG. 4. Variation of impurity susceptibility against temperature. The exactly screened case ($\delta = 0$) saturates to a constant value at low temperatures, indicating complete screening. The cases of inexact screening show a divergence of the susceptibility, which means there is a remnant local spin at the impurity. Since the axes are in log scale, the behaviour is $\log T \sim -\log\chi$ which translates to $\chi \sim 1/T$.

The χ is seen to diverge as T^{-1} at low temperatures. Such a non-analyticity in a response function is a signature of the critical nature of the Hamiltonian. This is in contrast to the behaviour in the non-critical exactly-screened fixed point where the ground state is unique. There, the susceptibility becomes constant at low temperatures: $\chi(T\to 0) = \frac{W}{4T_K}$, T_K being the single-channel Kondo temperature and W the Wilson number[10,40,67,82]. We have checked the case of general spin-S impurity numerically (fig. 4), and the general conclusion is that all exactly-screened models show a constant impurity susceptibility at $T \to 0$, while the over-screened and under-screened cases show a diverging impurity susceptibility

in the same limit. A similar divergence is also seen in the susceptibility of the outer spins, calculated by inserting a magnetic field purely on the outer spins.

A second non-analyticity arises when we consider the impurity free energy and the magnetization. The thermal free energy is given by

$$F(h) = -\frac{1}{\beta}\ln Z(h) = -\frac{1}{\beta}\ln\sum_{E_n} e^{-\beta E_n} \tag{19}$$

At $T \to 0$, only the most negative energy $E_{\min}$ survives. The minimal energy eigenvalue is

$$E_{\min} = -\frac{J}{4} - \frac{1}{2}\sqrt{J^2(K+1)^2/4 + h^2 + |h|J(K-1)} \tag{20}$$

The first derivative of the free energy with respect to the field gives

$$F'(h \neq 0, T \to 0) = -\frac{2h + J(K-1)\text{sign}(h)}{4\sqrt{\frac{J^2}{4}(K+1)^2 + h^2 + |h|J(K-1)}} \tag{21}$$

There we used the result that the derivative of $|x|$ is $\text{sign}(x)$. If we now take h to zero from both directions, we get the magnetization of the impurity

$$m = F'(h \to 0^{\pm}, T \to 0) = \mp\frac{1}{2}\frac{(K-1)}{(K+1)} \tag{22}$$

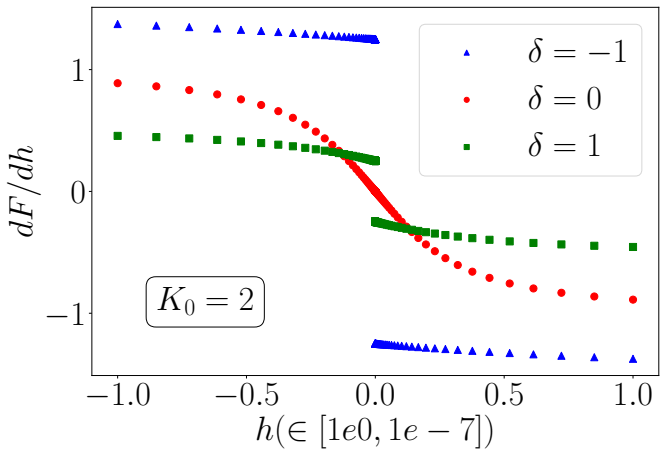

FIG. 5. Behaviour of the impurity magnetization for three values of $(K, 2S) = (2,4), (3,3), (4,2)$. Only the case of $K = 2S = 3$ ($\delta = 0$) is analytic near zero. The non-analyticity of the other cases arises because of the frustration brought about by the degeneracy of the star graph ground state.

The magnetization is therefore discontinuous as $h \to 0$; it goes to different values depending on the direction in which we take the limit. The non-analyticity for $K > 1$ occurs because there is at least one pair of ground state with non-zero parity π^z and magnetic field is able to flip one ground state into the state of opposite parity. This available space for scattering is simply the frustration that we discussed earlier. Indeed, we have checked numerically (see fig. 5) that the non-analyticity exists for all $\delta \neq 0$, where $\delta = \frac{K}{2} - S$ is the deviation from exact screening.

C. Topological properties of ground state manifold

We now present the non-local twist and translation operators which can be used to explore the degenerate ground state manifold of the star graph model. First we define two operators $\hat{T}$ and $\hat{O}$, which we will call the translation and twist operators respectively:

$$\hat{T} = e^{i\frac{2\pi}{K}\hat{\Sigma}}\ ,\ \hat{O} = e^{i\hat{\phi}}\ ,\ \ \hat{\Sigma} = [\hat{J}^z - (K-1)/2] \tag{23}$$

One can see that the generators of these above operators commute with the Hamiltonian, $[H, J^x] = [H, J^z] = [H, J^z] = 0$. In the large channel limit we can do semi-classical approximation. As J^x and J^y both commutes with the Hamiltonian H then $[H, J^y(J^x)^{-1}] = 0$, and any non-singular function of these operators must also commute with the Hamiltonian, thus we can say that

$$\hat{\phi} = \tan^{-1}(\hat{J}^y(\hat{J}^x)^{-1}) \tag{24}$$

Then we get $[\hat{\phi}, \hat{H}] = 0$. We can label the ground states by the eigenvalues of the translation operator $\hat{T}$. We can also use the ground states labeled by the eigenvalues of J^z (M, say). Then the ground states are

$$|M_1\rangle, |M_2\rangle, |M_2\rangle, \cdots, |M_K\rangle \tag{25}$$

Then the operations of the translation operators on this states are give below.

$$\hat{T}|M_i\rangle = e^{i\frac{2\pi}{K}[M_i - (K-1)/2]}|M_i\rangle = e^{i2\pi\frac{p_i}{K}}|M_i\rangle\ ,\ p_i \in [K] \tag{26}$$

Now we check the braiding rule between the twist and the translation operators, we find

$$\begin{aligned}\hat{T}\hat{O}\hat{T}^\dagger\hat{O}^\dagger &= e^{\frac{2\pi}{K}[i\hat{\Sigma}, i\hat{\phi}]} = e^{i\frac{2\pi}{K}} \\ \hat{T}\hat{O}^m\hat{T}^\dagger\hat{O}^{\dagger m} &= e^{\frac{2\pi}{K}[i\hat{\Sigma}, im\hat{\phi}]} = e^{i2\pi\frac{m}{K}}\end{aligned} \tag{27}$$

Next, we shown that the states $\hat{O}^m|M_i\rangle$ are orthogonal to each other and with the state $|M_i\rangle$.

$$\begin{aligned}\hat{T}\hat{O}^m|M_i\rangle &= \hat{O}^m\hat{T}e^{i2\pi\frac{m}{K}}|M_i\rangle = \hat{O}^m e^{i\frac{2\pi(m+p_i)}{K}}|M_i\rangle \\ \hat{T}\left(\hat{O}^m|M_i\rangle\right) &= e^{i\frac{2\pi(m+p_i)}{K}}\left(\hat{O}^m|M_i\rangle\right)\end{aligned} \tag{28}$$

Thus different states $\hat{O}^m|M_i\rangle$ for different m are labeled by different eigenvalues of the translation operations, thus are orthogonal to each other. Now as the twist operator $\hat{O}$ commutes with the Hamiltonian, thus we can see that

$$\langle M_i|\hat{O}^{m\dagger}H\hat{O}^m|M_i\rangle = \langle M_i|H|M_i\rangle \tag{29}$$

Thus the energy eigenvalues of all the orthogonal states are equal, which forms the K fold degenerate ground states. By the application of the twist operator $\hat{O}$ one can go from one degenerate ground states to another.

D. Local Mott liquid

By applying the unitary renormalization group method on the zero mode star graph Hamiltonian, we decouple the impurity spin from the zero-modes of the K channels:

$$H = \mathcal{J}\vec{S}_d.\sum_i \vec{S}_i = \mathcal{J}S^z_d S^z + \frac{\mathcal{J}}{2}(S^+_d S^- + S^-_d S^+)$$
$$H_D = \mathcal{J}S^z_d S^z \ , \quad H_X = \frac{\mathcal{J}}{2}(S^+_d S^- + S^-_d S^+) \qquad (30)$$

In order to remove the quantum fluctuations between the impurity spin and the rest, we perform one step of URG:

$$\Delta H = H_X(\hat{\omega} - H_D)^{-1}H_X \qquad (31)$$

The total bath spin operator S^z is not a good quantum number for the zero mode ground state, and because there is no net S^z field, the ground state manifold has a vanishing expectation value of S^z, $\langle S^z\rangle = 0$. We use this expectation value to replace the denominator of the above RG equation.

$$\beta_\uparrow(\mathcal{J},\omega_\uparrow) = (\mathcal{J}^2\Gamma_\uparrow)/2 \ , \quad \Gamma_\uparrow = (\omega_\uparrow - \mathcal{J}(S^z_d - 1))^{-1} \qquad (32)$$

Thus we get the effective Hamiltonian is

$$H_{eff} = \frac{\beta_\uparrow(\mathcal{J},\omega_\uparrow)}{4}(S^+S^- + S^-S^+) \qquad (33)$$

In terms of the electronics degree of freedom this looks

$$\frac{\beta_\uparrow(\mathcal{J},\omega_\uparrow)}{4} \sum_{\substack{i\neq j \\ \alpha_i,\beta_i\in\{\uparrow,\downarrow\} \\ \alpha_j,\beta_j\in\{\uparrow,\downarrow\}}} \vec{\sigma}_{\alpha_i\beta_i}\vec{\sigma}_{\alpha_j\beta_j} c^{(i)\dagger}_{0\alpha_i} c^{(i)}_{0\beta_i} c^{(j)\dagger}_{0\alpha_j} c^{(j)}_{0\beta_j} + \text{h.c.}$$

We will study the two cases of the above effective Hamiltonian depending on the sign of the prefactor. $\frac{\beta_\uparrow(\mathcal{J},\omega_\uparrow)}{2} > 0$ is the ferromagnetic case where, in the ground state, S takes the minimum value and S^z takes the maximum possible value. For an example, in the case of K channels the minimum value of S will be 0 or $1/2$ for K being *even* or *odd* respectively. We will be interested in the other case where $\frac{\beta_\uparrow(\mathcal{J},\omega_\uparrow)}{2} < 0$. In this case, the ground state is realised for S being maximum and S^z being minimum. The effective Hamiltonian can be re-written in this case as

$$H_{eff} = -|\beta_\uparrow(\mathcal{J},\omega_\uparrow)| \times (S^+S^- + S^-S^+)/4 \qquad (34)$$

The CSCO of this Hamiltonian contains H, S, S^z. In the ground state S is maximum thus $S = K/2$ and S^z can take $2S+1 = K+1$ values. Thus in the largest S sector there are $K+1$ states. By the application of twist operator $\hat{Q} = \exp(i\hat{\phi}\Phi/\Phi_0)$, where $\hat{\phi}$ is the conjugate to $S6z$ folloing the algebra $[\phi, \hat{S^z}] = i$, we get the twisted Hamiltonian

$$H(\Phi) = -\frac{|\beta_\uparrow(\mathcal{J},\omega_\uparrow)|}{2}S^2 + \frac{|\beta_\uparrow(\mathcal{J},\omega_\uparrow)|}{2}\left(S^z - \frac{\Phi}{\Phi_0}\right)^2 \qquad (35)$$

One can thus explore different S^z ground states via such flux tuning mechanism.

For a K channel star graph problem the ground state is K fold degenerate associated with different J^z values $\{-(K-1)/2, -(K-3)/2, \cdots, (K-1)/2\}$. After removing the quantum fluctuations between the impurity spin and the outer spins, we get an all-to-all model (eq.(35)) as the effective Hamltonian. The eigenstates of this all-to-all Hamiltonian can be labeled by the eigenvalues of S^z. There are $K+1$ such states made out of only the outer spins. The total state including the impurity spin can be written as $|J^z\rangle = |S^z_d\rangle \otimes |S^z\rangle$ labeled by $J^z = S^z_d + S^z$. As the all-to-all model has Z_2 symmetry in impurity sector, there are $2(K+1)$ total states. For $S^z_d = 1/2$, $\{J^z\} = \{-(K-1)/2, \cdots, (K-1)/2, (K+1)/2\}$ and for $S^z_d = -1/2$, $\{J^z\} = \{-(K+1)/2, -(K-1)/2, \cdots, (K-1)/2\}$. We can see that in both the cases, all K states of the star graph ground state manifold are present in spectrum of the all-to-all model, one of them being the ground state. Using the twist operator, we can cycle between the various states.

IV. LOCAL NON-FERMI LIQUID EXCITATIONS OF THE 2CK MODEL

A. Effective Hamiltonian

Here we start with the star graph Hamiltonian, which is the zero bandwidth model for the two-channel Kondo as obtained from the URG.

$$H^{(2)} = \mathcal{J}\vec{S}_d.(\vec{S}_1 + \vec{S}_2) \ , \quad \vec{S}_i = \frac{1}{2}\, c^\dagger_{i,\alpha}\ \vec{\sigma}_{\alpha,\beta}\ c_{i,\beta} \qquad (36)$$

Here, $\vec{S}_i = 1, 2$ represents the spin degree of freedom present at the origin of the i^{th} channel. This two channel Hamiltonian has $2^3 = 8$ states in the eigenspectrum[95]. There are two degnerate ground states labeled by $|J^z = \pm 1/2\rangle$ with energy $-\mathcal{J}$ and 6 excited states. We will now consider real space hopping between the zeroth site and the first site as a perturbation on top of the star graph Hamiltonian, and obtain the effective Hamiltonian for the excitations by accounting for this hopping using degenerate perturbation theory.

$$H_X = -t \sum_{\substack{<1,l_1> \\ <2,l_2>}} (c^\dagger_{1,\sigma} c_{l_1,\sigma} + c^\dagger_{2,\sigma} c_{l_2,\sigma} + \text{ h.c.}) \qquad (37)$$

Here l_i represents the nearest site to the origin of the i^{th} channel. The perturbation H_X contains scattering which takes the states of the zero mode Hamiltonian out of spin-channel scattering space. For simplicity we will be keeping only one neareast neighbor to the origin of each channel. Thus before we start the perturbation theory we must expand the basis of the zero mode Hamiltonian itself. The basis we are interested in is $\{\mathcal{B}_{extnd}\}$ given as

$$\{|S^z_{imp}, n_{1,\uparrow}, n_{1,\downarrow}, n_{2,\uparrow}, n_{2,\downarrow}\rangle \otimes |n_{l_1,\uparrow}, n_{l_1,\downarrow}, n_{l_2,\uparrow}, n_{l_2,\downarrow}\rangle\}$$

Note there are now $2^4 = 16$ elements in the subspace $\{|n_{l_1,\uparrow}, n_{l_1,\downarrow}, n_{l_2,\uparrow}, n_{l_2,\downarrow}\rangle\}$. In the spin-channel basis $\{\mathcal{B}\}$ there 2 degenerate ground states. Because the unperturbed Hamiltonian $\mathcal{H}_0$ has no scattering terms outside the spin sector, in the extended basis $\{\mathcal{B}_{extnd}\}$ the total ground state degeneracy becomes simply $2\times 2^4 = 32$-fold. Thus the total Hamiltonian we are interested in is

$$\mathcal{H} = \frac{\mathcal{J}\hbar}{2}\ \vec{S}_d.\sum_{i=\{1,2\}}\sum_{\alpha,\beta\in\{\uparrow,\downarrow\}} c^\dagger_{i\alpha}\vec{\sigma}_{\alpha\beta}c_{i\alpha} + H_X \quad (38)$$

In the expanded basis there are 32 degnerate states given as

$$|\tilde{\alpha}_0\rangle = |J^z = +1/2\rangle \otimes |n_{l_1,\uparrow}, n_{l_1,\downarrow}, n_{l_2,\uparrow}, n_{l_2,\downarrow}\rangle \quad (39)$$
$$|\tilde{\alpha}_1\rangle = |J^z = -1/2\rangle \otimes |n_{l_1,\uparrow}, n_{l_1,\downarrow}, n_{l_2,\uparrow}, n_{l_2,\downarrow}\rangle \quad (40)$$

The first order and the second order corrections to the low energy effective Hamiltonian are

$$H^{(1)} = \sum_{ij}|\alpha_i\rangle\langle\alpha_i|V|\alpha_j\rangle\langle\alpha_j|$$
$$H^{(2)} = \sum_{ij}\sum_l |\alpha_i\rangle\frac{\langle\alpha_i|V|\mu_l\rangle\langle\mu_l|V|\alpha_j\rangle}{E_0 - E_l}\langle\alpha_j| \ . \quad (41)$$

Here, $|\alpha_i\rangle$ represents the ground states with energy E_0 and μ_l represents the excited states with energy E_l. One can easily check that the diagonal contribution at any odd order is zero: the final state is never equal to the initial state. The off-diagonal part at first order is also zero. At second order we get both diagonal and off-diagonal contribitions to the effective Hamiltonian.

Total diagonal contribution is coming from the two states $|\tilde{\alpha}_0\rangle$ and $|\tilde{\alpha}_1\rangle$, individually fiven as $H^{(2)}_{diag}(1/2)$,$H^{(2)}_{diag}(-1/2)$ respectively.

$$H^{(2)}_{diag}(1/2) = \frac{2t^2}{E_0}\hat{I} - \Omega_l \ , \ H^{(2)}_{diag}(-1/2) = \frac{2t^2}{E_0}\hat{I} + \Omega_l \ (42)$$

where $S^z_{l_i} = (n_{l_i\uparrow} - n_{l_i\downarrow})/2$ and $\Omega_l = \frac{2t^2}{3E_0}(S^z_{l_1} + S^z_{l_2})$. Thus the total contribution to the diagonal effective Hamiltonian is $H^{(2)}_{diag} = -4t^2\hat{I}$, shows the absence of local Fermi liquid due to the exact cancellation of the field term. The off-diagonal contributio to the second order effective Hamiltonian is

$$\begin{aligned} H_{NFL} = H^{(2)}_{off} &= \sum_{i\neq j}\sum_l |\alpha_i\rangle\frac{\langle\alpha_i|V|\mu_l\rangle\langle\mu_l|V|\alpha_j\rangle}{E_0 - E_l}\langle\alpha_j| \\ &= -\frac{8t^2}{3}[(S^z_1)^2 c^\dagger_{2\uparrow}c_{2\downarrow}(c_{l_1\uparrow}c^\dagger_{l_1\downarrow} + c_{l_2\uparrow}c^\dagger_{l_2\downarrow}) \\ &+ (S^z_2)^2 c^\dagger_{1\uparrow}c_{1\downarrow}(c_{l_1\uparrow}c^\dagger_{l_1\downarrow} + c_{l_2\uparrow}c^\dagger_{l_2\downarrow})] + \text{h.c.} \ , \quad (43) \end{aligned}$$

The LEH is purely a non-Fermi liquid, arising due to the degenerate ground state manifold. Using this low energy effective Hamiltonian we have calculated different thermodynamic quatitites like susceptibility and specific heat. Both these measures shows logarithmic behavior at low temperature which is in agreement with known result in literature. These results are shown in the Supplementary material. In a similar way, we have calculated the LEH for the three channel Kondo. We find the absence of Fermi liquid in 2^{nd} order and the presence of non-Fermi liquid in the off-diagonal low energy effective Hamiltonian shown in the supplementary material.

B. Local marginal Fermi liquid and orthogonality catastrophe

The real space local low energy Hamiltonian that takes into account the excitations above the ground state is given by eq. 43 and can be written as

$$V_{\text{eff}} = \frac{2t^2}{\mathcal{J}^*}\left[\left(\sigma^z_{0,1}\right)^2 s^+_{0,2} + \left(\sigma^z_{0,2}\right)^2 s^+_{0,1}\right]\left(s^-_{1,1} + s^-_{1,2}\right) + \text{h.c.} \ ; \quad (44)$$

here, $\sigma^z_{0,l} = \hat{n}_{0\uparrow,l} - \hat{n}_{0\downarrow,l}$, $s^+ = c^\dagger_{0\uparrow,l}c_{0\downarrow,l}$ and $s^- = (s^+)^\dagger$. The notation $0\sigma, l$ has the site index $i = 0, 1, 2, \ldots$ as the first label, the spin index $\sigma = \uparrow, \downarrow$ as the second label and the channel index $l = 1, 2$ as the third index. Such non-Fermi liquid (NFL) terms in the effective Hamiltonian and the absence of any Fermi-liquid term at the same order should be contrasted with the local Fermi liquid excitations induced by the singlet ground state of the single-channel Kondo model[1,10,82]. We now take the MCK Hamiltonian to strong-coupling, and perform a perturbative treatment of the hopping. At $J \to \infty$, the perturbative coupling t^2/J is arbitrarily small and we again obtain Eq. 44. Such a change from the strong coupling model with parameter J to a weak coupling model with parameter t^2/J amounts to a duality transformation[84,85]. It can be shown that the duality transformation leads to an identical MCK model[84] (self-duality), which implies we can have identical RG flows, and our transformation simply extracts the NFL piece from the dual model. The self-duality also ensures that the critical intermediate-coupling fixed point is unique and can be reached from either of the models.

The diagonal part of eq. 44 is

$$V_{\text{eff}} = \frac{2t^2}{J}\sum_{l=1,2}\left(\sum_\sigma \hat{n}_{0\sigma,l}\right)s^+_{0,\bar{l}}s^-_{1,\bar{l}} + \text{h.c.} \quad (45)$$

where $\bar{l} = 3 - l$ is the channel index complementary to l. We will Fourier transform this effective Hamiltonian into $k-$space. The NFL part becomes

$$\sum_{\sigma,\{k_i,k'_i\},l}\frac{2t^2}{J}e^{i(k_1-k'_1)a}c^\dagger_{k\sigma,l}c_{k'\sigma,l}c^\dagger_{k_2\uparrow,\bar{l}}c_{k'_2\downarrow,\bar{l}}c^\dagger_{k_1\downarrow,\bar{l}}c_{k'_1\uparrow,\bar{l}} + \text{h.c.} \quad (46)$$

This form of the Hamiltonian is very similar to the three-particle interaction term in Appendix B of[70]. The channel indices in Eq. 46 can be mapped to the normal directions in[70]. The 2 particle-1 hole interaction in Eq. 46 has a diagonal component which can be obtained by setting

$k = k', k_1 = k_2'$ and $k_2 = k_1'$:

$$H_{\text{eff,MFL}} = \sum_{\substack{k,k_1,\\ k_2,\sigma,l}} \frac{2t^2 e^{i(k_1-k_2)a}}{J} \hat{n}_{k\sigma,l}\hat{n}_{k_2\uparrow,\bar{l}}\left(1-\hat{n}_{k_1\downarrow,\bar{l}}\right) + \text{h.c.}$$
$$= \sum_{\substack{k,k_1,\\ k_2,\sigma,l}} \frac{4t^2}{J}\cos a\,(k_1-k_2)\,\hat{n}_{k\sigma,l}\hat{n}_{k_2\uparrow,\bar{l}}\left(1-\hat{n}_{k_1\downarrow,\bar{l}}\right) \tag{47}$$

The most dominant contribution comes from $k_1 = k_2 = k'$, revealing the non-Fermi liquid metal[45,90]:

$$H^*_{\text{eff,MFL}} = \frac{4t^2}{J}\sum_{\sigma,k,k',l} \hat{n}_{k\sigma,l}\hat{n}_{k'\uparrow,\bar{l}}\left(1-\hat{n}_{k'\downarrow,\bar{l}}\right) \tag{48}$$

A non-local version of this effective Hamiltonian was found to describe the normal phase of the Mott insulator of the 2D Hubbard model, as seen from a URG analysis[70,71]. Following[70], one can track the RG evolution of the dual coupling $R_j = \frac{4t^2}{J_j}$ at the j^{rh} RG step, in the form of the URG equation

$$\Delta R_j = -\frac{R_j^2}{\omega - \epsilon_j/2 - R_j/8} \tag{49}$$

In the RG equation, ϵ_j represents the energy of the j^{th} isoenergetic shell. It is seen from the RG equation that R is relevant in the range of $\omega < \frac{1}{2}\epsilon_j$ that has been used throughout, leading to a fixed-point at $R^*/8 = \omega - \frac{1}{2}\epsilon^*$). The relevance of R is expected because the strong coupling J is irrelevant and $R \sim 1/J$.

The renormalisation in R leads to a renormalisation in the single-particle self-energy[70]. The $k-$space-averaged self-energy renormalisation is

$$\Delta\Sigma(\omega) = \rho R^{*2}\int_0^{\epsilon^*} \frac{d\epsilon_j}{\omega - \epsilon_j/2 + R_j/8} \tag{50}$$

The density of states can be approximated to be N^*/R^*, where N^* is the total number of states over the interval R^*. As suggested by the fixed point value of R_j, we can approximate its behaviour near the fixed point by a linear dependence of the dispersion ϵ_j. The two limits of the integration are the start and end points of the RG. We start the RG very close to the Fermi surface and move towards the fixed point ϵ^*. Near the start point, we substitute $\epsilon = 0$ and $R = \omega$, following the fixed point condition. From the fixed point condition, we also substitute $R^*/8 = \omega - \frac{1}{2}\epsilon^*$. On defining $\bar{\omega} = N^*\left(\omega - \frac{1}{2}\epsilon^*\right)$, we can write

$$\Delta\Sigma(\omega) \sim \bar{\omega}\ln\frac{N^*\omega}{\bar{\omega}} \tag{51}$$

The self-energy also provides the quasiparticle residue for each channel[70]:

$$Z(\bar{\omega}) = \left(2 - \ln\frac{2\bar{\omega}}{N^*\omega}\right)^{-1} \tag{52}$$

As $\omega \to 0$, the Z vanishes, implying that the ground state is not adiabatically connected to the Fermi gas in the presence of the NFL terms. This is the orthogonality catastrophe[96–99] in the two-channel Kondo problem, and it is brought about by the presence of the channel-non diagonal terms in Eq. 48. Such terms were absent in the single-channel Kondo model, because there was no multiply-degenerate ground state manifold that allowed scattering. This line of argument shows that the extra degeneracy of the ground state subspace and the frustration of the singlet order that comes about when one upgrades from the single-channel Kondo model to the MCK models is at the heart of the NFL behaviour, and the orthogonality catastrophe is expected to be a general feature of all such frustrated MCK models. A local NFL term and a similar self-energy was also obtained by Coleman, et al.[49] in terms of Majorana fermions at the strong-coupling fixed point of the $\sigma-\tau$ model, which they claimed was equivalent to the intermediate-coupling fixed point of the two-channel Kondo model. Along with the work by Schofield[39], this demonstration shows the universality between the two-channel Kondo and the $\sigma-\tau$ models.

V. ENTANGLEMENT PROPERTIES

A. Entanglement properties of the star graph

We will now show the results of our study of various entanglement measures in each of the K degenerate ground states $|J^z\rangle$ of a K channel star graph, labeled by the eigenvalues of J^z.

1. *Entanglement entropy between impurity and the rest*

In a single-channel Kondo model, the ground state is the unique singlet: $|J=0, J_z=0\rangle = \frac{1}{\sqrt{2}}\left(|\uparrow_d,\downarrow_0\rangle - |\downarrow_d,\uparrow_0\rangle\right)$, and the impurity entanglement entropy (EE_d) is at the maximum possible value of $\log 2$. We will now calculate the same quantify for the ground states $|J^z\rangle \equiv |S_d = 1/2, S = K/2; (S-1/2), J^z\rangle$ of the K channel model.

In order to compute EE_d for a particular state $|J^z\rangle$, we calculate the von-Neumann entropy of the reduced density matrix ρ_d obtained by partially tracing the associated density matrix $\rho = |J^z\rangle\langle J^z|$ over the impurity states:

$$\rho_d = \text{Tr}_d\rho = \sum_{S_d^z}\langle S_d^z|\rho|S_d^z\rangle\ , \quad EE_d = -\rho_d\log\rho_d \tag{53}$$

The EE_d for states of various J^z is shown as a function of the number of channels K in fig. 6. At a particular value of K on the $x-$axis, all the points parallel to the $y-$axis represent values of EE_d for various values of J^z in the ground state manifold of that particular value of K. The minimum entanglement entropy occurs in the

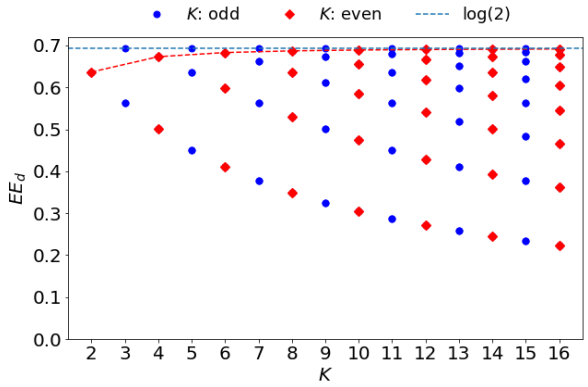

FIG. 6. Variation of impurity entanglement entropy (EE_d) with the rest for different channels (K). The maximum entropy in the large K limit is $\log 2$.

maximum J^z state ($|J^z = J\rangle$), and this minimum value decreases with increase in K. On the other hand, the maximum entanglement entropy is attained in the state with minimum J^z. This maximum value of the entanglement entopy is always $\ln 2$ for odd values of K; for even values of K, the value asymptotically reaches $\log 2$ at large K.

A very similar computation gives the entanglent entropy between one outer spin and the rest of the spins, and it is shown in Fig. 7. We again find that the minimum entanglement entropy is associated with the state $|J^z = J\rangle$ and it falls with increasing K, approaching zero asymptotically; the maximum entanglement entropy is, as before, associated with the state $|\,(J^z)_{\rm min}\rangle$ and it rises to $\log 2$ in the limit $K \gg 1$.

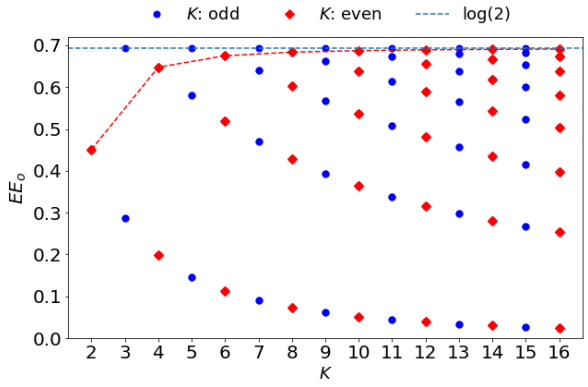

FIG. 7. Variation of the entanglement entropy of an outer spin (EE_o) with the rest for different channels (K). The maximum entanglement entropy in the large K limit is $\log 2$.

Two interesting features emerge from the study:

- For the odd K models, the impurity is maximally entangled with the other spins in the minimum J^z, $|J^z = 0\rangle$, member of the ground state manifold. At large K, the even K models also acquire this property, the minimum J^z there being $\pm\frac{1}{2}$.
- Both EE_d and EE_0 are individually equal for the states $|\pm J^z\rangle$, which shows that both types of entanglement entropy are invariant under the transformation $|J^z\rangle \to \pi\,|J^z\rangle$. This reflects a parity symmetry in the state space in terms of entanglement.

2. *Mutual Information*

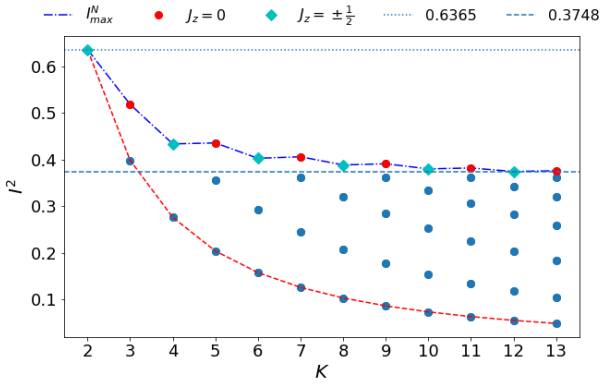

FIG. 8. Variation of mutual information ($I^2(d:o)$) with the rest for different channels K. The maximum mutual informaiton is saturating at 0.37.

Mutual information is a measure which captures the correlations present between two subsystems (A,B), in a particular state. It is defined as

$$I^2(A:B) = S_A + S_B - S_{A\cup B}\ , \tag{54}$$

where $S_{A(B)}$ is the von-Neumann entanglement entropy of the subsystem $A(B)$ with the rest, and $S_{A\cup B}$ is the von-Neumann entanglement entropy of A and B with the rest. We are interested in two types of mutual information: firstly, the mutual information $I^2(d:o)$ between the impurity and one of the other spins, and secondly, the mutual information $I^2(o:o)$ between any two of the outer spins. Both of these have been computed for various channel numbers K, and plotted in Figs. 8 and 9.

In both cases we find that the maximum and minimum mutual information are associated with the $|\,(J^z)_{\rm min}\rangle$ and $|J^z = J\rangle$ states respectively. We also find that the mutual information is the same in the states $|J^z\rangle$ and $\pi^x|J^z\rangle$, indicating the parity symmetry in the mutual information measure. In the large channel limit ($K \gg 1$), the maximum $I^2(d:o)$ and $I^2(o:o)$ saturate to the common value of 0.375.

3. *Multipartite information*

Similar to mutual information, one can calculate higher order multipartite information to study the nature of correlations present in different ground states. We define the

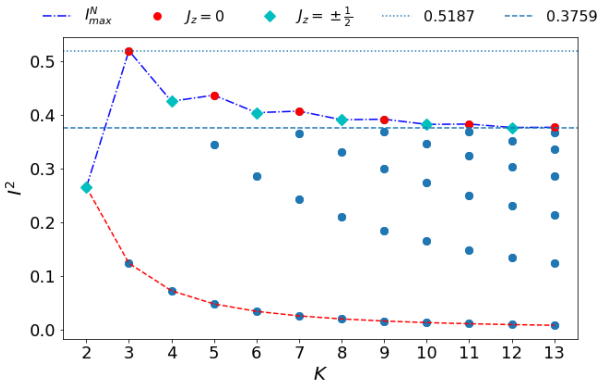

FIG. 9. Variation of mutual information $(I^2(o:o))$ with the rest for different channels (K). The minimum mutual inforamtion is vanishing in the large K limit.

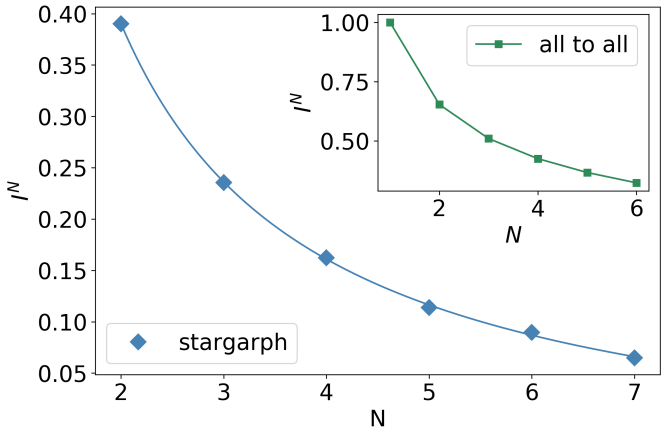

FIG. 10. Variation of multi-partite information I^N among the outer spins as a function of N for the multi channel case with $K = 8$. The inset shows the variation of the similar I^N vs N for an all-to-all model. Both show power law behavior.

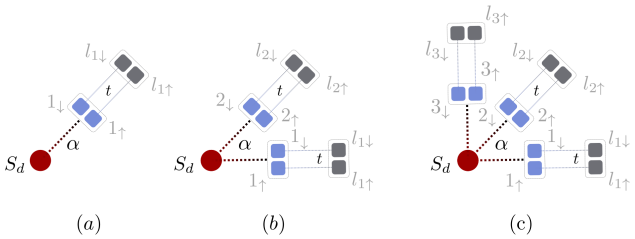

FIG. 11. This is a schematic diagram of (a) single channel and (b) two channel problem. S_d is the impurity spin. For more details refer to the text.

tripartite information among three subsystems A, B, C as $I^3_{ABC} = (S_A + S_B + S_C) - (S_{AB} + S_{BC} + S_{CA}) + S_{ABC}$. I^3 shows behavior similar to the mutual information - the highest I^2 value is associated with the $(J^z)_{\min}$ state and it saturates in the limit of $K \gg 1$. One can measure $N-$partite information for a collection of subsystems (CSS) $\{\mathcal{A}_N\} \equiv \{A_1, A_2, \cdots, A_N\}$. To define the $N-$partite information, we first define the power set of the CSS $\{\mathcal{A}_N\}$ as $\mathcal{P}(\{\mathcal{A}_N\})$, and the collection of all subsets of $\mathcal{P}(\{\mathcal{A}_N\})$ with m subsystems in it as $\mathcal{B}_m(\{\mathcal{A}_N\}) \equiv \{Q \mid Q \subset \mathcal{P}(\{\mathcal{A}_N\}), |Q| = m\}$. We also define the union and intersection of all the subsystems present in Q as $V_\cup(Q) \equiv \bigcup_{A\in Q} A$ and $V_\cap(Q) \equiv \bigcap_{A\in Q} A$ respectively. Finally, the von Neumann entanglement entropy of the subsystem A is given by S_A. Then the $N-$partite information that we are interested in is defined as

$$I^N_{\{\mathcal{A}_N\}} = \left[\sum_{m=1}^{N} (-1)^{m-1} \sum_{Q\in\mathcal{B}_m(\{\mathcal{A}\})} S_{V_\cup(Q)}\right] - S_{V_\cap(\mathcal{A}_N)} \quad (55)$$

Studying these multipartite information one can understand the nature of the multiparty correlations present among the outer spins. Our study of this multi-partite information presented in the above Fig. (10) shows that the higher order multi partite information (I^N) decreases as you increase the order (N) following a power law. In the inset of the Fig. 10 we have shown the similar I^N vs N behavior observed in the ground state of the all-to-all effective Hamiltonian (Eq.35). This similar power law behavior shows that one can capture the similar entanglement properties either from the star graph or from the corresponding all-to-all model.

B. Entanglement properties of the multi-channel Kondo fixed point

To understand the correlations present in the ground state of the MCK fixed point, we introduce excitations into the star graph ground state. We will work with the Hamiltonian Eq.(38) where we consider nearest-neighbor real space hopping t from the zeroth site into the lattice (Fig. 11). Setting $t = 0$ recovers the zero bandwidth version of the MCK. In the $K = 1$ single channel case, the impurity (S_d) is talking to the spin degree of freedom at the real space origin $(\{1_\uparrow, 1_\downarrow\})$ of the single conduction bath via a Heisenberg spin-exchange coupling. For $K = 2$, the impurity is interacting with 2 distinct local spins $\{1_\uparrow, 1_\downarrow\}$ and $\{2_\uparrow, 2_\downarrow\}$ belonging to zeroth sites of different conduction channels, and the real space hopping connects these zeroth sites to their nearest neighbor sites. For example, $\{1_\uparrow, 1_\downarrow\}$ gets linked to $\{l_{1\uparrow}, l_{1\downarrow}\}$. This amounts to saying that for a K channel model, we are solving a problem with one spin 1/2 degree of freedom and $2K$ lattice sites. As we increase the hopping strength t from zero to non-zero, the zeroth sites start interacting with their respective nearest neighbor sites.

1. *Impurity entanglement entropy*

The impurity entanglement entropy $EE_d(t)$ in the ground state is shown as a function of t in Fig. 12 for three

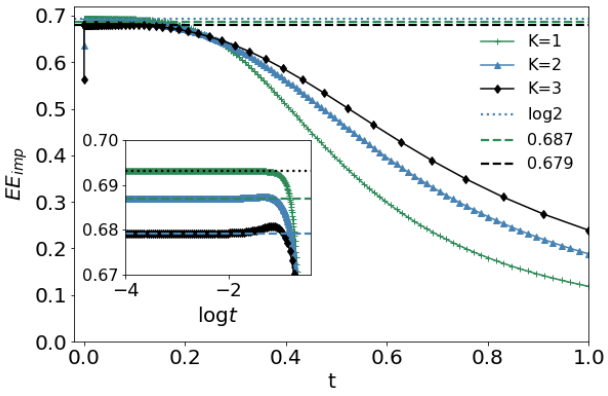

FIG. 12. This Figures shown the variation of impurity entanglement entropy EE_{imp} with the variation of the hopping strangth t for three different channel cases, $K = 1, 2, 3$.

values of channel number K. At low hopping strength ($0 < t \ll 1$), EE_d is independent of t and achieves a constant value. This value decreases with increasing K. On the other hand this order of EE_d changes at high t strength, where higher the channel number higher the impurity entanglement entropy. Though the impurity entanglement entropy at low hopping strength is very close to each other for different channels, the single channel impurity entanglement entropy varies smoothly with the increase of t from zero to nonzero value without any discontinuity. On the other hand for higher channels like $K = 2$ and $K = 3$ there is a discontinuity in the impurity entanglement entropy at $t = 0^+$.

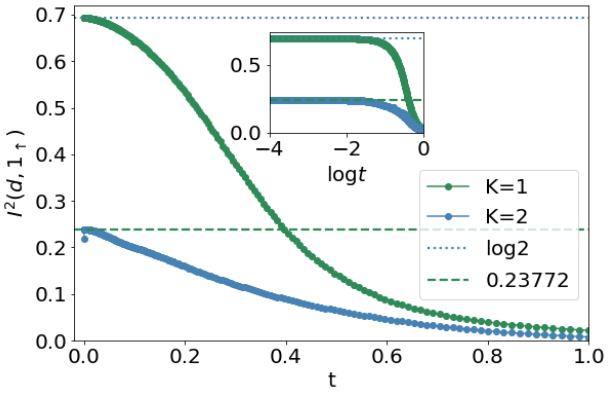

FIG. 13. This figure show the variation of mutual information between the impurity spin and $1_\uparrow$ state with respect to the variation of the hopping strength t. For more details please refer to the text. The errorbar σ_2 of the two channel data at low hopping strength $\sigma_2 \approx 0.002$.

2. *Intra-channel Mutual information*

Here we are interested in calculating Mutual information between two Fock states in the ground state wavefunction as a function of the hopping strength t varying from 0 to non zero values.

Case 1: First, we study the mutual information between the impurity spin S_d and $1_\uparrow$ Fock state (Fig. 11) represented as $MI(d, 1\uparrow)$, where 1 is realspace origin of the 1^{st} conduction channel. For single channel case this $1_\uparrow$ site can be chosen uniquely but for K channel cases there are K possible choices, due to the symmetry any one choice will show similar mutual information signature. Similarly due to the $SU(2)$ spin rotation symmetry the mutual information between the impurity spin and $1_\downarrow$ state will not be any different. We have numerically computed the variation of mutual information with respect to the hopping strength t and presented in the Fig. 13. As shown in the inset of the Fig. 13 at low hopping strength the mutual information for both the single channel and twochannel cases is saturating at different values. In the single channel case the Mutual information for $t = 0$ is $MI(d, 1_\uparrow) = \log 2$ and changes smoothly to nozero t values, similar to the previous impurity entanglement entropy study (EE_{imp}).

$$S_d = S_{1_\uparrow} = S_{d,1_\uparrow} = \log 2\ ,\ MI(d, 1_\uparrow) = \log 2 \quad (56)$$

This $\log 2$ value shows the stability of the zero mode of single channel and perfect screening. Next we focus to the two channel case where the mutual information is $MI(d, 1_\uparrow) = 0.2401$ which is less than the single channel case showing the breakdown of screening. Note, unlike the single channel case there is a discontinuity in $MI(d, 1_\uparrow)$ at $t = 0^+$.

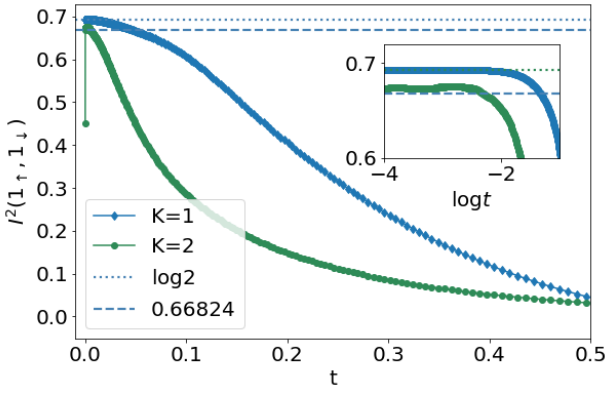

FIG. 14. This figure shows the variation of mutual information ($i^2(1_\uparrow, 1_\downarrow)$) among the two fock states present on the realspace origin (1) of a conduction channel with the hopping strength t. The errorbar σ_2 for the two channel at low hopping strength is $\sigma_2 \approx 0.013$.

Case 2: Similarly we have computed the mutual information $MI(1_\uparrow, 1_\downarrow)$ (Fig. 14) which measures intra chan-

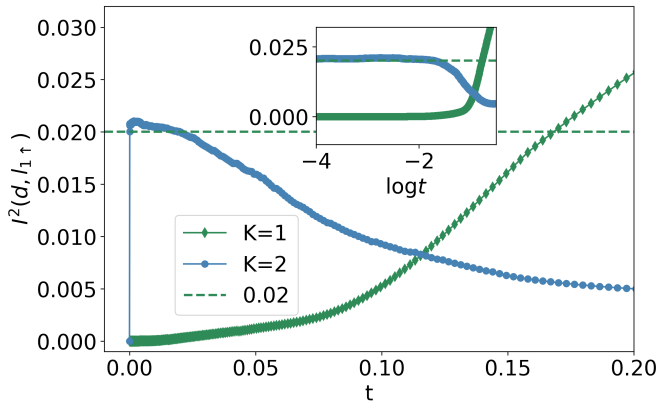

FIG. 15. Variation of the mutual information $MI(d, l_{1\uparrow})$ between the impurity spin and the $l_{1\uparrow}$ Fock state as a function of hopping strength t. The errorbar σ_2 for the two channel case is $\sigma_2 \approx 0.001$.

nel mutual information beteen two fock states $1_\uparrow, 1_\downarrow$ present at realspace origin. We find that the Mutual information is a smooth function of t for single channel and for two channel there is a discontinuity at $t = 0^+$. Note, $MI(1_\uparrow, 1_\downarrow) > MI(d, 1_\uparrow)$ for all t values show the presence of stronger intra-site correlation.

Case 3: Here we measure mutual information between the impurity and the Fock state of the nearest neighbor site to the realspace origin (Fig. 11) of the conduction channel, $MI(d, l_{1\uparrow})$ as shown in the Fig. 15. Vanishing mutual information for the single channel case shows the perfect screening of the impurity spin. On the other had we expect the breakdown of screening in two channel case, which is confirmed by the non-zero value of mutual information at small t values. Here also we find a dicontinuity inthe mutual information at $t = 0^+$.

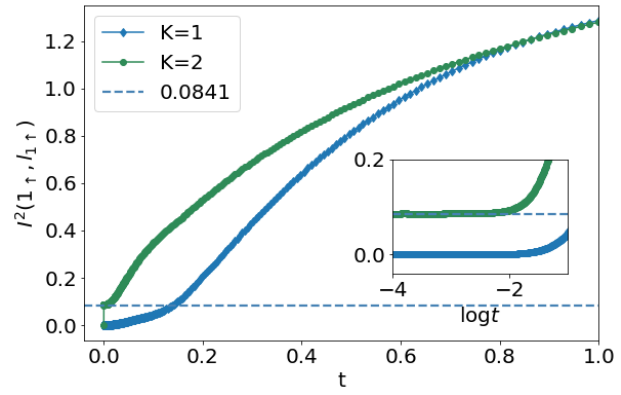

FIG. 16. Variation of the mutual information $MI(1_\sigma, l_{1\sigma})$ between two nearest neighbor sites as function of the hopping strength. The errorbar for the two channel case is $\sigma_2 \approx 0.005$.

Case 4: Another complementary study can be made by measuring the mutual information between conduction channel realspace origin and it's nearest neighbor site to check their mutual entanglement. As shown in the Fig. 16, we find that at low hopping strength the single channel mutual information vanishes showing the decoupling of those two states. On the other hand in the two channel case there is a nonzero mutual information which verifies the presence of active scattering between the local Mott liquid and the local non-Fermi liquid phases. Similar discontinuity in the mutual information was observed at $t = 0^+$. Apart form the above mutual information

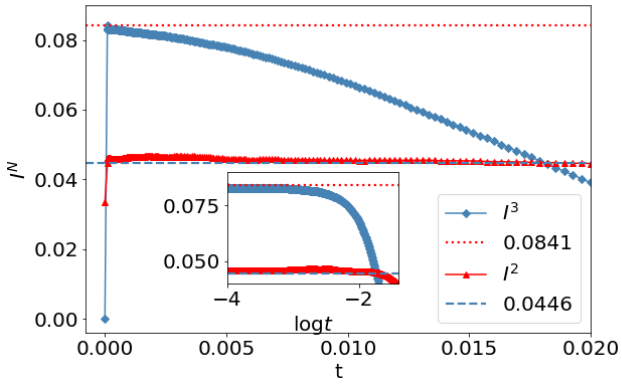

FIG. 17. Red: This is the Mutual information $I^2(1_\uparrow, 2_\uparrow)$ and the Blue is the tripartite infrmation $I^3(1_\uparrow, l_{1\uparrow}, l_{1\downarrow})$. The errorbar ($\sigma$) for the I^3 and I^2 near the low hopping strength are 0.002 and 0.003 respectively.

studies we have computed the intra-channel tripartite information $I^3(1_\uparrow, l_{1\uparrow}, l_{1\downarrow})$ of the two-channel ground state which measuring the correlation present among those three Fock states (Fig. 17(blue)) which show that there is a discontinuity in the triparite information at $t = 0^+$ and at low hopping strength the tripartite information is independent of t with a value 0.084. This non-zero value of tripartie information supports the presence of non-Fermi liquid with more than two-particle correlation within. We have also studied inter-channel mutual informaition $I^2(1_\uparrow, 2_\uparrow)$ for this two channel case as shown in the (Fig. 17(red)). This suggest the presence of correlation and quantum entanglement between these two channels supporting the presence of all-to-all local mott liquid.

3. *Bures distance and orthogonality catathrope*

Apart from different entanglement measures we have measured the Bures distance, which is a measure of distance between two density matrices. Which is defined as

$$d_{Bures}(\rho_1, \rho_2) = \sqrt{2}\left[1 - \mathrm{Tr}\left\{\left(\rho_1^{1/2}\rho_2\rho_1^{1/2}\right)^{1/2}\right\}\right] \quad (57)$$

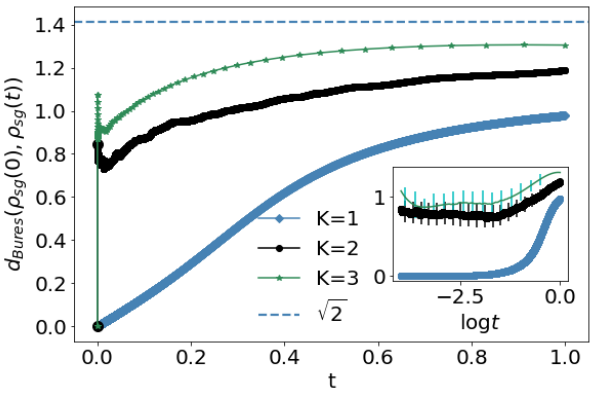

FIG. 18. Variation of Bures distance between the reduced denisty matrix of star graph at $t = 0$ and $t \neq 0$ with the variation of hopping strength t. The errorbar (σ) of the two channel and three channel data are 0.14 and 0.08 respectively, and near $t \approx 1$ the σ is 0.04 and 0.07 respectively.

One can see from the above defination that, the maximum and minimum distance it can have is $\sqrt{2}$ and 0 respectively. This measure represents the distance between two states in a Hilbert space.

We get the ground state wavefunction of the problem by solving the Hamiltonian Eq.(38) $|\psi(t)\rangle$ which is a function of t and $\rho(t) = |\psi(t)\rangle\langle\psi(t)|$. We are interested in the reduced density matrix of the star graph sites, to get that we partial trace out all other nearest neighbor sites, $\rho_{sg}(t) = \mathrm{Tr}_{NN}(\rho(t))$. Then the Bures distance between the reduced denisty matrices $\rho_{sg}(t = 0)$ and $\rho_{sg}(t)$, denoted as $d_{Bures}(\rho_{sg}(t = 0), \rho_{sg}(t))$ are computed for single, two and three channel cases.

We have shown the variation of the Bures distance as a function of the hopping strength in the Fig. 18 above. For all three cases the Bures distance is zero at $t = 0$, whic is obvious. But as you turn on t slightly there is a discontinuity in the distance for two and theree channel cases against the single channel where the distance varies smoothly. This discontinuity in the higher channel case against the single channel is similar to all the above entanglement studies. The smooth variation of the distance in the single channel case shows the adiabatic continuation of the reduced stargarph density matrix from the $t = 0$ case to $t \neq 0$ case. On the other had the abrupt jump in the Bures distance for higher-channel cases at $t = 0^+$ shows the breakdown of adiabatic continuity siganling an orthogonality catastrophe. Three channel case show higher amoount of discontinuity than the two channel case saturating at higher value for $t = 1$. Due to finite size system we cannot see the exact orthogonality by getting the $d_{Bures} = \sqrt{2}$, but higher channel cases with higher discontinuity suggests so.

All the above entanglement studies suggest that for two channel problem there is a discontinuity in the ground state at $t = 0^+$, whereas for the single channel case it is a smooth function. Thus for single channel case the $t = 0$ and $t \neq 0$ cases can be adiabtically connected, which is not the case for any other channel cases.

VI. DUALITIES OF THE MULTI-CHANNEL KONDO MODEL

We start from a strong coupling ($J \to \infty$) spin-S impurity MCK Hamiltonian in the over-screened regime ($K > 2S$),

$$H(J) = \sum_{k,\sigma,l} \epsilon_{k,l} \hat{n}_{k\sigma,l} + J \vec{S}_d \cdot \vec{S} \ . \tag{58}$$

Here, $\vec{S}$ is the total spin $\sum_l \sum_{kk'\alpha\beta} \vec{\sigma}_{\alpha\beta} c^\dagger_{k\alpha,l} c_{k'\beta,l}$ of all the zero modes. At strong coupling, the ground states of the star graph eq. 8 act as a good starting point for a perturbative expansion. As argued previously, there are $K - 2S_d + 1$ ground states, labeled by the K values of the total spin angular momentum $J^z = S^z_d + S^z = -\frac{K}{2} + S_d, -\frac{K}{2} + S_d + 1, \ldots, \frac{K}{2} - S_d$. Since a general spin-$s$ object is simply a $2s+1$ level system, the $K-$fold degenerate ground state manifold can be used to define a new impurity spin $\mathbb{S}_d$ of multiplicity $2\mathbb{S}_d + 1 = K - 2S_d + 1$ which implies that we need $\mathbb{S}_d = \frac{K}{2} - S_d$. That is, the spin-$S_d$ impurity has a dual described by a spin-$(K - 2S_d + 1)$ impurity. The states of this new spin are defined by

$$\begin{aligned} \hat{\mathbb{S}^z_d} \left|S^z\right\rangle &= S^z \left|S^z\right\rangle, \\ \hat{\mathbb{S}^\pm_d} \left|S^z\right\rangle &= \sqrt{\mathbb{S}_d \left(\mathbb{S}_d + 1\right) - S^z \left(S^z \pm 1\right)} \left|S^z \pm 1\right\rangle \end{aligned} \tag{59}$$

While the ground state subspace gives rise to the new central spin object, the excited states of the star graph can be used to define bosonic operators that mediate interactions between the central spin and the next-nearest neighbour lattice sites[84]. In terms of the zero-bandwidth spectrum, the bosonic operators represent scattering between the ground state subspace and the excited subspaces. Through a Schrieffer-Wolff transformation in the small coupling $\frac{t^2}{J}$, one can then remove this interaction and generate an exchange-coupling between the new impurity $\vec{\mathbb{S}}_d$ and the new zero modes formed out of the remaining sites in the lattice[84] (by remaining, we mean those real space sites that have not been consumed into forming the new spin). The new Hamiltonian, characterized by the small super-exchange coupling $\mathbb{J}$ of the general form $\gamma t^2/J$, has the form

$$H'(\mathbb{J}) = \sum_{k,\sigma,l} \epsilon_{k,l} \hat{n}_{k\sigma,l} + \mathbb{J} \vec{\mathbb{S}_d} \cdot \vec{\mathbb{S}} \tag{60}$$

$\vec{\mathbb{S}}$ is the local bath spin formed by the new zero modes. This Hamiltonian is very similar to the one in eq. 58, and that is the essence of the strong-weak duality: One can go from the over-screened strong coupling spin-S MCK model to another over-screened weak coupling spin-$(K-$

$2S+1$) MCK model. For the case of $K=4S$, we have $\mathbb{S}_d = S_d$, and both S_d and $\mathbb{S}_d$ describe the same spin objects (at least formally). The two models are then said to be self-dual. For example, for the case of spin-half MCK model, two-channel model is self-dual.

One important consequence of the duality relationship between the two over-screened models is that the RG equations are also dual; while the strong coupling model has an irrelevant coupling $\mathcal{J}$ that flows down to the intermediate fixed point $\mathcal{J}^*$, the weak coupling model has a relevant coupling $\mathbb{J}$ that flows up to the same fixed point $\mathbb{J}^* = \mathcal{J}^*$. From the RG equation for the general spin-S MCK model, we know that $\mathbb{J}^* = \frac{2}{K\rho'}$, where ρ' is the DOS for the bath of the weak coupling Hamiltonian. This constrains the form of the scaling factor γ:

$$\mathbb{J}^* = \frac{\gamma 4t^2}{\mathcal{J}^*} = \frac{2}{K\rho'} \implies \gamma = \frac{1}{4t^2}\mathcal{J}^{*2} = \frac{1}{K^2t^2\rho\rho'} \quad (61)$$

There exists another set of dual points in the MCK model. This was hinted at when we looked at the degree of compassion in eq. 12. Since Γ depends only on the magnitude of δ, both $\pm\delta$ will give the same degree of compensation, same ground state energy and same ground state degeneracy $\left(g_K^{S_d} = |\delta| + 1\right)$. The definition of δ gives the duality transformation as $K \to 2S_d, S_d \to \frac{K}{2}$. That is, we transform from a $K-$channel MCK model with spin-S_d impurity, to a $2S_d$-channel MCK with a spin-$\frac{K}{2}$ impurity. The exactly-screened model $K = 2S_d$ maps on to itself and is therefore self-dual under this transformation.

For $K \neq 2S_d$, we transform an over-screened model into an under-screened model and vice versa. This duality relationship allows us to infer the RG scaling behaviour of one of the models if we know that of the other. If we know that for a certain pair of values K and S_d, the $K-$channel MCK model with spin-S_d impurity has an intermediate fixed point, we can immediately conclude that the $2S_d$-channel spin-$\frac{K}{2}$ model has a strong coupling fixed point.

VII. QUANTUM PHASE TRANSITION IN THE MULTI-CHANNEL KONDO MODEL UNDER CHANNEL ANISOTROPY

For a channel anisotropic MCK model with K Kondo couplings $\mathcal{J}_i$ for each fo the K conduction channels, the zero bandwidth model is

$$H_K(\vec{\mathcal{J}}) = \sum_{i=1}^{K} \mathcal{J}_i \vec{S}_d.\vec{S}_i \quad (62)$$

For the special case $\mathcal{J}_i = \mathcal{J}, \forall i$ we get the usual isotropic star graph model. For the case of spin-1/2 impurity, we find that the Hamiltonian with any value of $\mathcal{J}_i > 0$ has K fold ground state degeneracy. This shows that the ground state degeneracy of the star graph model is extremely robust against the channel anisotropy; the ground state degeneracy does not change until at least one $\mathcal{J}_i$ vanishes.

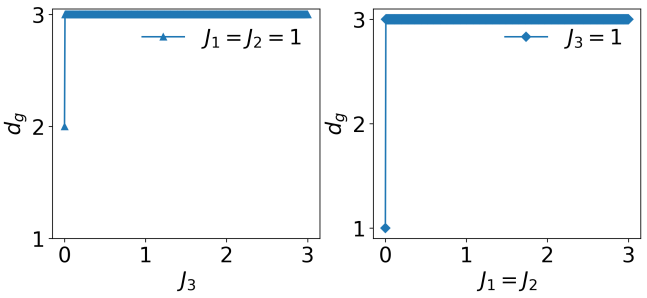

FIG. 19. *Left:* Shows the variation of the ground state degeneracy with the variation of the coupling J_3 keeping other two couplings $J_1 = J_2 = 1$ fixed. *Right:* Variation of ground state degeneracy with the variation of the couplings $J_1 = J_2$ keeping theJ_3 = fixed. Both these show the robustness of the ground state degeneracy against the channel anisotropy.

We have demonstrated this numerically for a three channel anisotropic star graph model. In Fig. 19(a), we show that if two couplings are kept fixed to be equal ($\mathcal{J}_1 = \mathcal{J}_2 = 1$) and the third coupling $\mathcal{J}_3$ is tuned from some finite value to zero, the degeneracy does not change from 3 to 2 until $\mathcal{J}_3$ becomes zero. At that point, the model becomes a two channel Kondo problem. We also show in Fig. 19(b) that we keep the first coupling $\mathcal{J}_3$ fixed to 1 and vary the common coupling $\mathcal{J}_1 = \mathcal{J}_2$ from non-zero to zero, this is equivalent to keeping $\mathcal{J}_1 = \mathcal{J}_2 = 1$ fixed and taking $\mathcal{J}_1$ to infinity from finite. In this case we find when the coupling $\mathcal{J}_1 = \lambda_2 = 0$ the degeneracy becomes one showing the effective single channel nature.

The above demonstration makes it clear that the ground state degeneracy can change only when at least one of the Kondo couplings vanish. This can be realised under RG flow if one considers the anisotropic MCK model.

$$H = \sum_{k,\alpha,l} \epsilon_{k,l}\hat{n}_{k\alpha,l} + \sum_{\substack{kk',\\ \alpha,\beta,l}} \mathcal{J}_l \vec{S}_d \cdot \frac{1}{2}\vec{\sigma}_{\alpha\beta} c^\dagger_{k\alpha,l} c_{k'\beta,l} \ . \quad (63)$$

We consider the specific case where $K-1$ channels have the same coupling $\mathcal{J}_1 = \mathcal{J}_2 = ... = \mathcal{J}_{K-1} = \mathcal{J}_+$ and the remaining channel has a different coupling $\mathcal{J}_K = \mathcal{J}_-$. The RG equations for such a model are

$$\frac{\Delta\mathcal{J}_\pm}{|\Delta D|} = -\frac{\mathcal{J}_\pm^2\rho}{\mathcal{D}_\pm} + \frac{\rho^2\mathcal{J}_\pm}{2}\left[\frac{(K-1)\mathcal{J}_+^2}{\mathcal{D}_+} + \frac{\mathcal{J}_-^2}{\mathcal{D}_-}\right] , \quad (64)$$

where $\mathcal{D}_\pm = \omega - \frac{D}{2} - \frac{\mathcal{J}_\pm}{4}$ are the denominators of the URG equations. Setting $\mathcal{J}_+ = \mathcal{J}_-$ leads to the critical fixed point at $\mathcal{J}_+^* = \mathcal{J}_-^* = \mathcal{J}_* = \frac{2}{K\rho}$. We now perturb around this fixed point by defining new variables $j_\pm = \mathcal{J}_\pm - \mathcal{J}_*$. We also assume that the bandwidth is large enough so that $\mathcal{D}_\pm \simeq \omega - \frac{D}{2} - \frac{\mathcal{J}_*}{4} = -|\mathcal{D}_*|$. Performing a linear stability analysis about $j_\pm = 0$ then reveals the following two possibilities:

(a) If $j_- < 0, j_+ > 0$, the deviation j_- is relevant and $\mathcal{J}_-$ flows to zero. The flow of j_+ are constrained such that the remaining couplings $\mathcal{J}_+$ flow to the stable intermediate fixed point of the $K-1$ channel MCK model: $J_{+,*} = \frac{2}{(K-1)\rho}$.

(b) If $j_- > 0, j_+ < 0$, the couplings $\mathcal{J}_+$ are irrelevant, and this leads to a single channel Kondo model described by the coupling $\mathcal{J}_-$ which flows to strong coupling.

These conclusions show that the K channel intermediate fixed point is unstable under channel anisotropy[14,32,37,45]. If one of the couplings becomes smaller than the rest, then that coupling flows to zero while the other $K-1$ couplings flow to the $K-1$ channel fixed point. On the other hand, if $K-1$ couplings are smaller than a single coupling, then the smaller couplings vanish while the remaining coupling flows to strong-coupling.

VIII. CONCLUSIONS

In summary, we have explored the low-energy behaviour of the multi-channel Kondo models using the unitary renormalization group (URG) method and obtained a better understanding of the role of ground state degeneracy and quantum-mechanical frustration in shaping the non-Fermi liquid physics and criticality. Using the unitary renormalization group technique, we have obtained the zero-temperature phase diagram of the MCK problem and an effective Hamiltonian with a simple zero bandwidth limit - the star graph, and it determines the ground state energy, wavefunction and degeneracy of the MCK models. This star graph is found to explain much of the physics of overscreening and criticality, including the singularities in the susceptibility and magnetisation, as well as a reduction in the degree to which the impurity spin is compensated. The overarching message there was that the ground state degeneracy of the star graph (which is unity for single-channel and greater for the overscreened models) was the key ingredient in leading to the qualitative and quantitative differences from the single-channel model The presence of ground state degeneracy also allows the construction of non-local twist operators and fractional excitations in the ground state manifold. Integrating out the quantum fluctuations of the impurity leads to an all-to-all effective Hamiltonian for the local bath spins, and the Hamiltonian is foudn to contain inter-channel quantum scattering in terms of electron-hole pairs, theryby creating a local Mott-liquid phase at the origin of the lattice.

The low energy effective Hamiltonian (LEH) for the excitations is then obtain by considering fluctuations of the conduction bath on top of the ground state. The LEH for the 2-channel Kondo confirms absence of any Fermi liquid phase due to an exact cancellation across the ground state manifold, and the presence of inter-channel off-diagonal non-Fermi liquid terms. Our analysis reinforces the idea that the ground state degeneracy is crucial to the non-Fermi liquid physics and to the presence of such off-diagonal terms in the LEH. The existence of a marginal Fermi liquid within the effective Hamiltonian clearly displays the orthogonality catastrophe in the form of singularities that are absent at exact screening. Studies of various thermodynamic properties (presented in the supplementary material) from this 2-channel Kondo LEH like specific heat and susceptibility show logarithmic dependence at low temperature, in agreement with the literature[8,30–35,42–46].

The non-diagonal nature of the LEH is further investigated through the several measures of entanglement. The entanglement entropy, calculated from the minimum J^z states, between the impurity and the outer spins, as well as between an outer spin and the rest saturate to $\ln 2$ in the large channel limit saturate. The opposite behaviour happens in the maximum J^z state, where the entanglement entropy decreases with the increase of channel number. The large values of inter-channel mutual information indicate high inter-channel correlation in the MCK ground state. The power-law dependence of the multipartite information among the outer spins of the star graph model is similar to the power-law behavior of the all-to-all local Mott-liquid ground state. The presence of a discontinuity in the non-Fermi liquid ground state multi-channel entanglement as compared to the smooth behaviour in the single-channel counterpart again points to the orthogonality catastrophe in the low-energy phase of the multi-channel models. Higher discontinuity for a higher number of channels was observed in the Bures distance study.

The URG study of the channel anisotropic MCK shows the critical and unstable nature of the isotropic fixed point; under any anisotropic perturbations, the RG flows go towards either the single-channel model or the symmetric MCK with one less channel coupled to the impurity. This is complemented by the study of the star graph ground state degeneracy which shows that the degeneracy changes only if one or more couplings vanishes. When combined, we can conclude that in the presence of channel anisotropy, the degeneracy of the MCK ground state does not change until the RG reaches the stable fixed point.

This method serves as a template for the study of other quantum impurity systems. We have already seen that the degeneracy of the star graph is robust under anisotropy; one can perform similar studies in the presence of a superconducting gap that cuts off the ground state manifold from the excitations, hence providing the degeneracy a topological protection. The duality transformations then allow us to view the topologically protected ground state as a larger quantum spin which is essentially isolated. This holds immense potential for applications in quantum information and quantum computation. More fine-tuned behaviour can be obtained by studying the MCK model with an easy-axis anisotropy term $\left(J^i\right)^2$ along one of the axes (i). Such a term would, if it is able to survive the RG flows towards low energy,

lift the degeneracy of the ground state and make it possible to achieve perfect screening even with $K > 2S_d$. One can also study the multi-channel lattice models[100,101] to better understand the role played by singlet frustration and ground state degeneracy in the competition between the local moment versus the heavy fermion sea.

ACKNOWLEDGMENTS

SP and Anirban Mukherjee thanks the CSIR, Govt. of India and IISER Kolkata for funding through a research fellowship. Abhirup Mukherjee thanks IISER Kolkata for funding through a research fellowship. SL thanks · · · ·.

* sp14ip022@iiserkol.ac.in
† am18ip014@iiserkol.ac.in
‡ mukherjee.anirban.anirban@gmail.com
§ slal@iiserkol.ac.in

[1] A. C. Hewson, The Kondo Problem to Heavy Fermions (Cambridge University Press, 1993).
[2] P. W. Anderson and G. Yuval, Physical Review Letters **23**, 89 (1969).
[3] P. W. Anderson, G. Yuval, and D. Hamann, Physical Review B **1**, 4464 (1970).
[4] P. W. Anderson, Journal of Physics C: Solid State Physics **3**, 2436 (1970).
[5] K. G. Wilson, Rev. Mod. Phys. **47**, 773 (1975).
[6] N. Andrei, K. Furuya, and J. H. Lowenstein, Rev. Mod. Phys. **55**, 331 (1983).
[7] A. M. Tsvelick and P. B. Wiegmann, Adv. in Phys. **32**, 453 (1983).
[8] I. Affleck and A. W. Ludwig, Physical Review B **48**, 7297 (1993).
[9] I. Affleck, Acta Phys.Polon.B **26** (1995).
[10] P. Nozieres, Journal of Low Temperature Physics **17**, 31 (1974).
[11] A. C. Hewson, Advances in Physics **43** (1994).
[12] J. Kondo, Progress of Theoretical Physics **32**, 37 (1964), https://academic.oup.com/ptp/article-pdf/32/1/37/5193092/32-1-37.pdf.
[13] Y. hui Zhang, S. Kahle, T. Herden, C. Stroh, M. Mayor, U. Schlickum, M. Ternes, P. Wahl, and K. Kern, Nature Communications **4** (2013), 10.1038/ncomms3110.
[14] Nozières, Ph. and Blandin, A., J. Phys. France **41**, 193 (1980).
[15] I. Affleck and A. W. W. Ludwig, Phys. Rev. Lett. **68**, 1046 (1992).
[16] I. Affleck, A. W. W. Ludwig, and B. A. Jones, Phys. Rev. B **52**, 9528 (1995).
[17] A. Georges and Y. Meir, Phys. Rev. Lett. **82**, 3508 (1999).
[18] G. Zaránd, C.-H. Chung, P. Simon, and M. Vojta, Phys. Rev. Lett. **97**, 166802 (2006).
[19] A. K. Mitchell, D. E. Logan, and H. R. Krishnamurthy, Phys. Rev. B **84**, 035119 (2011).
[20] A. K. Mitchell, E. Sela, and D. E. Logan, Phys. Rev. Lett. **108**, 086405 (2012).
[21] E. J. König, P. Coleman, and Y. Komijani, Phys. Rev. B **104**, 115103 (2021).
[22] P. Coleman, Phys. Rev. B **35**, 5072 (1987).
[23] A. J. Millis and P. A. Lee, Phys. Rev. B **35**, 3394 (1987).
[24] A. Auerbach and K. Levin, Phys. Rev. Lett. **57**, 877 (1986).
[25] T. M. Rice and K. Ueda, Phys. Rev. B **34**, 6420 (1986).
[26] G. R. Stewart, Rev. Mod. Phys. **56**, 755 (1984).
[27] M. Granath and H. Johannesson, Phys. Rev. B **57**, 987 (1998).
[28] A. Zawadowski, Phys. Rev. Lett. **45**, 211 (1980).
[29] D. L. Cox and A. Zawadowski, Advances in Physics **47**, 599 (1998), https://doi.org/10.1080/000187398243500.
[30] I. Affleck and A. W. Ludwig, Nuclear Physics B **360**, 641 (1991).
[31] A. W. W. Ludwig and I. Affleck, Phys. Rev. Lett. **67**, 3160 (1991).
[32] I. Affleck, A. W. W. Ludwig, H.-B. Pang, and D. L. Cox, Phys. Rev. B **45**, 7918 (1992).
[33] O. Parcollet and A. Georges, Phys. Rev. Lett. **79**, 4665 (1997).
[34] I. Affleck, Journal of the Physical Society of Japan **74**, 59 (2005), https://doi.org/10.1143/JPSJ.74.59.
[35] V. J. Emery and S. Kivelson, Phys. Rev. B **46**, 10812 (1992).
[36] D. G. Clarke, T. Giamarchi, and B. I. Shraiman, Phys. Rev. B **48**, 7070 (1993).
[37] G. Zaránd and J. von Delft, Phys. Rev. B **61**, 6918 (2000).
[38] J. von Delft, G. Zaránd, and M. Fabrizio, Phys. Rev. Lett. **81**, 196 (1998).
[39] A. J. Schofield, Phys. Rev. B **55**, 5627 (1997).
[40] R. Bulla, T. A. Costi, and T. Pruschke, Rev. Mod. Phys. **80**, 395 (2008).
[41] H. B. Pang and D. L. Cox, Phys. Rev. B **44**, 9454 (1991).
[42] N. Andrei and C. Destri, Phys. Rev. Lett. **52**, 364 (1984).
[43] A. M. Tsvelick and P. B. Wiegmann, Zeitschrift für Physik B Condensed Matter **54**, 201 (1984).
[44] A. M. Tsvelick, Journal of Physics C: Solid State Physics **18**, 159 (1985).
[45] N. Andrei and A. Jerez, Phys. Rev. Lett. **74**, 4507 (1995).
[46] G. Zaránd, T. Costi, A. Jerez, and N. Andrei, Phys. Rev. B **65**, 134416 (2002).
[47] A. M. Sengupta and A. Georges, Phys. Rev. B **49**, 10020 (1994).
[48] M. Fabrizio, A. O. Gogolin, and P. Nozières, Phys. Rev. Lett. **74**, 4503 (1995).
[49] P. Coleman, L. B. Ioffe, and A. M. Tsvelik, Phys. Rev. B **52**, 6611 (1995).
[50] M. Fabrizio, A. O. Gogolin, and P. Nozières, Phys. Rev. B **51**, 16088 (1995).

[51] A. V. Rozhkov, International Journal of Modern Physics B **12**, 3457 (1998), https://doi.org/10.1142/S0217979298002805.
[52] R. Zheng, R.-Q. He, and Z.-Y. Lu, Phys. Rev. B **103**, 045111 (2021).
[53] K. Vladár and A. Zawadowski, Phys. Rev. B **28**, 1564 (1983).
[54] T. Cichorek, A. Sanchez, P. Gegenwart, F. Weickert, A. Wojakowski, Z. Henkie, G. Auffermann, S. Paschen, R. Kniep, and F. Steglich, Phys. Rev. Lett. **94**, 236603 (2005).
[55] D. C. Ralph and R. A. Buhrman, Phys. Rev. Lett. **69**, 2118 (1992).
[56] D. C. Ralph, A. W. W. Ludwig, J. von Delft, and R. A. Buhrman, Phys. Rev. Lett. **72**, 1064 (1994).
[57] Z. Iftikhar, S. Jezouin, A. Anthore, U. Gennser, F. D. Parmentier, A. Cavanna, and F. Pierre, Nature **526**, 233 (2015).
[58] L. J. Zhu, S. H. Nie, P. Xiong, P. Schlottmann, and J. H. Zhao, Nature Communications **7**, 10817 (2016).
[59] R. M. Potok, I. G. Rau, H. Shtrikman, Y. Oreg, and D. Goldhaber-Gordon, Nature **446**, 167 (2007).
[60] A. J. Keller, L. Peeters, C. P. Moca, I. Weymann, D. Mahalu, V. Umansky, G. Zaránd, and D. Goldhaber-Gordon, Nature **526**, 237 (2015).
[61] V. Emery and S. Kivelson, Nature **374**, 434 (1995).
[62] H. T. Mebrahtu, I. V. Borzenets, H. Zheng, Y. V. Bomze, A. I. Smirnov, S. Florens, H. U. Baranger, and G. Finkelstein, Nature Physics **9**, 732 (2013).
[63] B. Alkurtass, A. Bayat, I. Affleck, S. Bose, H. Johannesson, P. Sodano, E. S. Sørensen, and K. Le Hur, Phys. Rev. B **93**, 081106 (2016).
[64] D. Kim, J. Shim, and H.-S. Sim, Phys. Rev. Lett. **127**, 226801 (2021).
[65] A. Mukherjee and S. Lal, Nuclear Physics B **960**, 115170 (2020).
[66] A. Mukherjee and S. Lal, Nuclear Physics B **960**, 115163 (2020).
[67] A. Mukherjee, A. Mukherjee, N. S. Vidhyadhiraja, A. Taraphder, and S. Lal, arxiv (2021), arXiv:2111.10580 [cond-mat.str-el].
[68] S. Pal, A. Mukherjee, and S. Lal, **21**, 023019 (2019).
[69] S. P. Anirban Mukherjee and S. Lal, Journal of High Energy Physics **2021** (2021), 10.1007/JHEP04(2021)148.
[70] A. Mukherjee and S. Lal, New Journal of Physics **22**, 063007 (2020).
[71] A. Mukherjee and S. Lal, New Journal of Physics **22**, 063008 (2020).
[72] S. Patra and S. Lal, Phys. Rev. B **104**, 144514 (2021).
[73] J. Gan, **6**, 4547 (1994).
[74] E. Kogan, Journal of Physics Communications **2**, 085001 (2018).
[75] Y. Kuramoto, The European Physical Journal B - Condensed Matter and Complex Systems **5**, 457 (1998).
[76] A. M. Tsvelick and P. B. Wiegmann, Zeitschrift für Physik B Condensed Matter **54**, 201 (1984).
[77] A. K. Mitchell, M. R. Galpin, S. Wilson-Fletcher, D. E. Logan, and R. Bulla, Phys. Rev. B **89**, 121105 (2014).
[78] V. Tripathi, Landau Fermi Liquids and Beyond (CRC Press, 2018).
[79] E. Fradkin, Field theories of condensed matter physics (Cambridge University Press, 2013).
[80] C. M. Varma and Y. Yafet, Phys. Rev. B **13**, 2950 (1976).
[81] K. Yosida, Phys. Rev. **147**, 223 (1966).
[82] K. G. Wilson, Reviews of Modern Physics **47**, 773 (1975).
[83] C. P. Moca, I. Weymann, M. A. Werner, and G. Zaránd, Phys. Rev. Lett. **127**, 186804 (2021).
[84] C. Kolf and J. Kroha, Phys. Rev. B **75**, 045129 (2007).
[85] R. Žitko and M. Fabrizio, Phys. Rev. B **95**, 085121 (2017).
[86] J. Gan, N. Andrei, and P. Coleman, Phys. Rev. Lett. **70**, 686 (1993).
[87] A. M. Tsvelick and P. B. Wiegmann, Journal of Statistical Physics **38**, 125 (1985).
[88] T. Kimura and S. Ozaki, Journal of the Physical Society of Japan **86**, 084703 (2017), https://doi.org/10.7566/JPSJ.86.084703.
[89] D. Bensimon, A. Jerez, and M. Lavagna, Phys. Rev. B **73**, 224445 (2006).
[90] D. L. Cox and M. Jarrell, **8**, 9825 (1996).
[91] P. Coleman and C. Pépin, Phys. Rev. B **68**, 220405 (2003).
[92] N. Roch, S. Florens, T. A. Costi, W. Wernsdorfer, and F. Balestro, Phys. Rev. Lett. **103**, 197202 (2009).
[93] A. Schiller and L. De Leo, Phys. Rev. B **77**, 075114 (2008).
[94] P. Durganandini, EPL (Europhysics Letters) **95**, 47003 (2011).
[95] K. Tandon, S. Lal, S. K. Pati, S. Ramasesha, and D. Sen, Phys. Rev. B **59**, 396 (1999).
[96] C. Varma, Z. Nussinov, and W. Van Saarloos, Physics Reports **361**, 267 (2002).
[97] P. W. Anderson, Phys. Rev. Lett. **18**, 1049 (1967).
[98] K. Yamada and K. Yosida, Progress of Theoretical Physics **59**, 1061 (1978), https://academic.oup.com/ptp/article-pdf/59/4/1061/5315849/59-4-1061.pdf.
[99] K. Yamada and K. Yosida, Progress of Theoretical Physics **62**, 363 (1979).
[100] C. A. Piguet, D. F. Wang, and C. Gruber, Journal of Low Temperature Physics **106**, 3 (1997).
[101] M. Shaw, X.-w. Zhang, and D. Jin, Phys. Rev. B **57**, 8381 (1998).